
PASS: Ambiguity Guided Subsets for Scalable Classical and Quantum Constrained Clustering

Pedro Chumpitaz-Flores¹, My Duong¹, Ying Mao², Kaixun Hua¹

¹University of South Florida ²Fordham University

Abstract

Pairwise-constrained clustering augments unsupervised partitioning with side information by enforcing must-link (ML) and cannot-link (CL) constraints between specific samples, yielding labelings that respect known affinities and separations. However, ML and CL constraints add an extra layer of complexity to the clustering problem, with current methods struggling in data scalability, especially in niche applications like quantum or quantum-hybrid clustering. We propose PASS, a pairwise-constraints and ambiguity-driven subset selection framework that preserves ML and CL constraints satisfaction while allowing scalable, high-quality clustering solution. PASS collapses ML constraints into pseudo-points and offers two selectors: a constraint-aware margin rule that collects near-boundary points and all detected CL violations, and an information-geometric rule that scores points via a Fisher–Rao distance derived from soft assignment posteriors, then selects the highest-information subset under a simple budget. Across diverse benchmarks, PASS attains competitive SSE at substantially lower cost than exact or penalty-based methods, and remains effective in regimes where prior approaches fail.

1 Introduction

Clustering is a fundamental task in unsupervised learning, aiming to identify cohesive and distinct groups within datasets (Jain, 2010). A central objective of clustering is to find the optimal cluster assignment, referred to as the Minimum Sum-of-Squares Criteria (MSSC) (Späth, 1980). Nevertheless, purely unsupervised clustering algorithms often produce results misaligned with domain-specific insights or practical requirements (Basu et al., 2008; Brieden et al.,

2017). Incorporating prior knowledge as must-link (ML) and cannot-link (CL) constraints turns clustering into a semi-supervised task that improves interpretability and relevance (Tian et al., 2021; Yang et al., 2022). However, these constraints introduce new challenges: clusters may violate locality assumptions, undermining standard k -means, and constrained MSSC is NP-hard (Basu et al., 2008; Brieden et al., 2017). Heuristic solutions exist but suffer from initialization sensitivity and feasibility issues (Lloyd, 1982); subsequent refinements optimize assignment order (Tan et al., 2010), add constraint-aware auxiliary centroids (Huang et al., 2008), or defer constraint enforcement (Nghiem et al., 2020). At the same times, exact methods like (Aloise et al., 2009; Piccialli et al., 2022; Chumpitaz-Flores et al., 2025a) prioritize the solution quality of MSSC at the cost of scalability and have not been well-studied for pairwise constraints, as datasets with more than a thousand samples quickly become intractable for these algorithms.

Data subsampling with coresets or uncertain subset emerges as another approach that balances between scalability and solution quality. Coreset methods compress data to high-sensitivity regions so that any constraint-respecting solution evaluated on the summary approximates its cost on the full set (Schmidt and Wargalla, 2021; Huang et al., 2025). Ambiguity-based methods operationalize this balance by concentrating soft penalties (Basu et al., 2004) or oracle queries (Xu et al., 2005; Xiong et al., 2016) on uncertain points to reduce the complexity of the clustering formulation and resolve violations with minimal work (Xiong et al., 2016).

Moreover, from the quantum computing perspective, data subsampling is particularly advantageous when extending corresponding clustering algorithms to their quantum version, because shrinking the pairwise interaction graph directly reduces the embedding and annealing overhead incurred when dense logical couplings are mapped onto sparse annealing topologies (Könz et al., 2021). This approach mitigates the quadratic resource scaling that otherwise constrains problem size

on current hardware (Mirkarimi et al., 2024a; Glover et al., 2019). Consequently, the ambiguity-driven paradigm provides a pathway to handle the dense constraint graphs that challenge quantum annealing approaches (Tomesh et al., 2021a; Qu et al., 2022).

Our Contributions: We propose PASS, a scalable framework for pairwise-constrained k -means. First, we show that collapsing each ML component into a weighted pseudo-point produces a smaller MSSC instance with identical optima. We then optimize only on a feasibility-preserving working set that concentrates on CL violations and cluster intersections using information-geometric selectors. The reduction enables scalability beyond state-of-the-art classical heuristics and exposes a compact $\mathcal{O}(|S|k)$ QUBO, enabling hybrid quantum refinement that surpass current state of the art quantum clustering algorithm. Empirically, PASS delivers competitive or better SSE with substantially lower runtime, particularly in datasets where classical penalty methods and quantum-hybrid clustering fail to scale.

2 Related Works

Minimum Sum-of-Squares Criteria (MSSC) (Späth, 1980), is a central objective in clustering. A widely-used adaptation for MSSC under constraints is Constrained k -Means (Wagstaff et al., 2001), which modifies standard assignments to avoid violating constraints but struggles with initialization sensitivity and feasibility issues (Piccialli et al., 2022; Xu and Lange, 2019). To address these, heuristic variants have been proposed: ICOP- k -means (Tan et al., 2010; Rutayisire et al., 2011) optimizes assignment order; MLC- k -means (Huang et al., 2008) utilizes assistant centroids; and methods that enforce constraints post initial clustering (Nghiem et al., 2020).

By compressing data into small, constraint-aware coresets, previous algorithms can achieve near-optimal, constraint-respecting solutions that scale to very large datasets. Bhattacharya et al. (2018) showed that constrained k -means outputs a small list of candidate center sets so that one is a $(1 + \varepsilon)$ -approximation, shifting complexity from data size n to dependence on k and enabling reductions that underlie later coreset constructions. Schmidt and Wargalla (2021) prove that in low-dimensional Euclidean space, one can compute coresets that are constraint-agnostic: any assignment pairwise constraint checkable by an oracle is preserved up to $(1 + \varepsilon)$ on the coreset, giving data-size-efficient summaries for constrained k -means. (Braverman et al., 2021) introduced a uniform-sampling meta-theorem that reduces constrained clustering to “ring” instances, yielding uniformly sampled coresets (often

with size independent of n). Nevertheless, cannot-link requirement, especially hard CL collapses the additivity assumption and blows up point sensitivities, thus inflates the coreset to linear size.

Research on constrained clustering allocates computation to where assignments are fragile or constraint-laden, but operationalizations differ. Penalty-based methods such as PCKMeans and related formulations encode must-link and cannot-link relations as soft terms in the objective, permitting limited violations while steering optimization toward feasibility (Basu et al., 2004; Davidson and Ravi, 2005). These models implicitly emphasize boundary or conflicting assignments because those accrue higher penalties, yet they do not isolate a dedicated working subset. Query-efficient strategies instead identify points near decision boundaries or in overlapping regions, obtain a small number of pairwise labels from an oracle, and then re-cluster with the augmented constraint set; examples include selecting boundary cases from spectral eigenvectors (Xu et al., 2005) and actively choosing points that reduce uncertainty in the spectral embedding (Xiong et al., 2016). Assignment-repair procedures address constraint pressure directly: PCCC adjusts candidate labels for points generating the largest constraint-violation penalties and propagates updates through the constraint graph; empirically, it scales to datasets with up to 60,000 samples (Baumann and Hochbaum, 2024).

Scalability proves to be particularly challenging for clustering with both quantum and quantum-hybrid frameworks, especially when constraints are involved. Despite progress in quantum clustering without constraints, only a handful of recent small-scale annealer-based proofs of concept tackle pairwise constraints (Seong and Park, 2025; Cohen et al., 2020). We establish the effectiveness of our method by extending it to a quantum-hybrid clustering pipeline, leveraging QUBO’s natural ability to encode must-/cannot-link constraints as quadratic couplings between binary assignment variables, yielding compact, feasible instances with stable penalty schedules and materially improved scalability over naive encodings.

3 Pairwise-Constrained k -Means

3.1 Problem Formulation

Given a dataset $X = \{x_1, \dots, x_i\} \subset \mathbb{R}^d$ with S samples and d features, the MSSC problem with pairwise constraints aims to find k clusters that minimize the Sum of Squared Errors (SSE) while satisfying must-

link (ML) and cannot-link (CL) constraints:

$$\min_b \sum_{i \in \mathcal{S}} \sum_{k \in \mathcal{K}} b_{i,k} \|x_i - \mu_k\|^2 \quad (1a)$$

$$\text{s.t. } b_{i,k} = b_{i',k}, \quad \forall (i, i') \in \mathcal{T}_{ml}, k \in \mathcal{K}, \quad (1b)$$

$$b_{i,k} + b_{i',k} \leq 1, \quad \forall (i, i') \in \mathcal{T}_{cl}, k \in \mathcal{K}, \quad (1c)$$

$$b_{i,k} \in \{0, 1\}, \quad \forall i \in \mathcal{S}, k \in \mathcal{K}. \quad (1d)$$

where $i \in \mathcal{S} := \{1, \dots, S\}$ is the sample index, $k \in \mathcal{K} := \{1, \dots, K\}$ is the cluster index, and $\mu = [\mu_1, \dots, \mu_K]$ with $\mu_k \in \mathbb{R}^d$ represents each cluster center. The binary variable $b_{i,k}$ takes 1 when x_i is assigned to cluster k and 0 otherwise. The sets $\mathcal{T}_{ml} \subseteq \mathcal{S} \times \mathcal{S}$ and $\mathcal{T}_{cl} \subseteq \mathcal{S} \times \mathcal{S}$ specify pairs that must or must not be in the same cluster, respectively. The pairwise-constrained MSSC can thus be formulated as the following SSE minimization problem:

$$\min_{\mu, d, b} \sum_{i \in \mathcal{S}} d_{i,*} \quad (2a)$$

$$\text{s.t. } -N(1 - b_{i,k}) \leq d_{i,*} - d_{i,k} \leq N(1 - b_{i,k}) \quad (2b)$$

$$d_{i,k} \geq \|x_i - \mu_k\|_2^2 \quad (2c)$$

$$\text{Constraints 1b - 1d} \quad (2d)$$

Here $d_{i,k}$ is the distance between x_i and μ_k , $d_{i,*}$ is the distance from x_i to its assigned centroid, and N is a big- M constant. Define $d_i = [d_{i,1}, \dots, d_{i,K}, d_{i,*}]$, $d = [d_1, \dots, d_S]$, $b_i = [b_{i,1}, \dots, b_{i,K}]$, $b = [b_1, \dots, b_S]$. Constraint (2b) links $d_{i,*}$ and $d_{i,k}$ when $b_{i,k} = 1$.

3.2 Cost-Equivalent MSSC with Must-Link Collapse

We adopt the must-link collapse from Chumpitaz-Flores et al. (2025a). In our implementation, each must-link component is represented by a single weighted pseudo-point, rather than by repeated pseudo-samples.

Let $\mathcal{C} = \{x_1, \dots, x_p\}$ be a cluster with centroid μ . Assume x_1, \dots, x_t form a must-link component $\mathcal{C}_{ml} \subseteq \mathcal{C}$. Define

$$\mu_{ml} = \frac{1}{t} \sum_{i=1}^t x_i, \quad \text{tr}(\Sigma_{ml}) = \frac{1}{t-1} \sum_{i=1}^t \|x_i - \mu_{ml}\|^2,$$

and set $\text{tr}(\Sigma_{ml}) = 0$ when $t = 1$. Let $\hat{\mathcal{C}}$ be obtained by replacing \mathcal{C}_{ml} with a pseudo-representation at μ_{ml} . Then

$$\text{sse}_{\mathcal{C}}(\mu) = \text{sse}_{\hat{\mathcal{C}}}(\mu) + (t-1)\text{tr}(\Sigma_{ml}), \quad (3)$$

as shown in Chumpitaz-Flores et al. (2025a).

Let $\{\mathcal{C}_{ml}^{(j)}\}_{j \in J}$ be the must-link components in X with sizes t_j , centroids $\mu_{ml}^{(j)}$, and traces $\text{tr}(\Sigma_{ml}^{(j)})$. We form the collapsed dataset

$$\hat{X} = (X \setminus R) \cup \bigcup_{j \in J} \{(\mu_{ml}^{(j)}, w_j = t_j)\}, \quad R = \bigcup_{j \in J} \mathcal{C}_{ml}^{(j)}.$$

Let $\hat{\mathcal{S}}$ index \hat{X} . The resulting cost-equivalent problem is

$$\min_{\mu, d, b} \sum_{i \in \hat{\mathcal{S}}} w_i d_{i,*} + \sum_{j \in J} (t_j - 1) \text{tr}(\Sigma_{ml}^{(j)}), \quad (4a)$$

$$\text{s.t. } \text{Constraints 2b and 2c.} \quad (4b)$$

The second term in (4a) is constant with respect to (μ, b) , so minimizers of (4) correspond to minimizers of the ML-only restriction of Problem (2) under the component-to-pseudo mapping.

Mixed ML and CL constraints. With both ML and CL constraints, we first contract each ML component to obtain \hat{X} with only CL constraints. We then apply our subset restriction to points involved in cannot-link interactions or with uncertain assignments.

4 Subset Selection Techniques

Reduce the effective problem size by directing computation to points with assignment ambiguity and to those participating in cannot-link conflicts. There also exist points whose assignments are stable under the current model, for instance when they lie far from decision boundaries. The main computational effort arises instead around ambiguous assignments and violated constraints. By focusing optimization on this subset, we aim to obtain computational savings while maintaining feasibility under our construction.

4.1 Constraint-Aware Subset Selection

We focus computation on a subset $S \subset \mathcal{S}$ with $|S| \ll |\mathcal{S}|$ while preserving feasibility of cannot-link constraints. Let g^* denote a fixed baseline assignment such as unconstrained k -means.

Definition 1 (Ambiguity and Constraint Sets). For each point $x_i \in S$, define the signed margin

$$m(i) = \min_{g \neq g^*(i)} \left(\|x_i - \mu_{g^*(i)}\|^2 - \|x_i - \mu_g\|^2 \right).$$

Values $m(i) > 0$ indicate that there exists a cluster that improves the current assignment, values $m(i) < 0$ indicate that the current cluster is closer than any

alternative, and values near zero indicate ambiguity. We mark ambiguity with a positive threshold τ as

$$\text{Amb}(i) = \mathbb{I}[m(i) > -\tau],$$

so that clearly misassigned points with $m(i) > 0$ and near-boundary points with $-\tau < m(i) \leq 0$ are included.

The cannot-link violation set under g^* is

$$V = \{i \in \mathcal{S} : \exists j \in \mathcal{S} \text{ such that } (i, j) \in \mathcal{T}_{cl} \text{ and } g^*(i) = g^*(j)\}.$$

Threshold Selection The margin threshold τ is set as the p -th percentile of the empirical distribution $\{m(i)\}_{i \in \mathcal{S}}$ shifted toward zero. Typical values are $p \in [10, 30]$ to capture points near decision boundaries while avoiding an overly large subset.

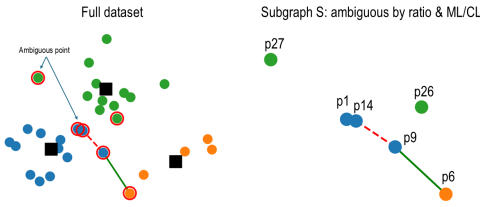


Figure 1: Subset selection with $k = 3$. Left: original data with ambiguous points in red and cannot-links as dashed red edges. Right: induced subproblem on S with the constraint graph.

Definition 2 (Reduced Working Subset). We select

$$S = V \cup \{i \in \mathcal{S} : \text{Amb}(i) = 1\}.$$

This set captures both constraint violations and points with ambiguous assignments. The construction is made explicit in Algorithm 1.

On S , we optimize

$$\min_d \sum_{i \in S} \sum_{g \in \mathcal{K}} \Delta_{i,g} d_{i,g} \quad (5)$$

$$\text{s.t. } \sum_{g \in \mathcal{K}} d_{i,g} = 1, \quad \forall i \in S \quad (6)$$

$$d_{u,g} + d_{v,g} \leq 1, \quad \forall (u, v) \in \mathcal{T}_{cl} \cap (S \times S), \quad \forall g \in \mathcal{K} \quad (7)$$

$$d_{u,g^*(v)} = 0, \quad \forall (u, v) \in \mathcal{T}_{cl} \text{ with } u \in S, v \notin S \quad (8)$$

$$d_{i,g} \in \{0, 1\}, \quad \forall i \in S, \forall g \in \mathcal{K}, \quad (9)$$

where $\Delta_{i,g} = \|x_i - \mu_g\|^2 - \|x_i - \mu_{g^*(i)}\|^2$, $\Delta_{i,g^*(i)} = 0$.

Proposition 3 (Feasibility Preservation). Any solution feasible for (6)–(8) extends to a feasible solution of the full problem by fixing assignments outside S to g^* .

Proof. Constraints inside S are enforced by (7). For edges that connect one endpoint in S and one endpoint outside S , constraint (8) forbids assigning the endpoint in S to the cluster of the fixed endpoint outside S . If a cannot-link constraint were violated entirely outside S , then one endpoint would belong to V by definition, which contradicts $V \subseteq S$. \square

Algorithm 1 Constraint-Aware Subset Selection

Require: Dataset X , current centroids $\{\mu_g\}$, constraints \mathcal{T}_{cl} , percentile $p \in [10, 30]$

Ensure: Subset $S \subseteq \mathcal{S}$

```

1: Compute baseline assignment  $g^*(i)$  for all  $i \in \mathcal{S}$   $\triangleright$ 
   e.g., via  $k$ -means
2: Initialize  $V \leftarrow \emptyset$ ,  $m \leftarrow []$   $\triangleright$  Violation set and
   margins array
3: for each point  $i \in \mathcal{S}$  do
4:    $d_{\text{current}} \leftarrow \|x_i - \mu_{g^*(i)}\|^2$ 
5:    $d_{\text{next}} \leftarrow \min_{g \neq g^*(i)} \|x_i - \mu_g\|^2$ 
6:    $m[i] \leftarrow d_{\text{current}} - d_{\text{next}}$   $\triangleright$  Signed margin
7: end for
8: for each constraint  $(i, j) \in \mathcal{T}_{cl}$  do
9:   if  $g^*(i) = g^*(j)$  then  $\triangleright$  Constraint violation
10:     $V \leftarrow V \cup \{i, j\}$ 
11:   end if
12: end for
13:  $\tau \leftarrow p$ -th percentile of  $\{m[i]\}_{i \in \mathcal{S}}$   $\triangleright$  Shift toward
   zero
14:  $A \leftarrow \{i \in \mathcal{S} : m[i] > -\tau\}$   $\triangleright$  Ambiguous points
15:  $S \leftarrow V \cup A$ 
16: return  $S$ 

```

4.2 Information-Geometric Subset Selection

While the constraint-aware selection in Section 4.1 ensures feasibility, we can further improve selection quality by incorporating statistical uncertainty measures. We now introduce an information-geometric approach that refines the subset using Fisher–Rao geometry to maximize statistical information content.

Definition 4 (Fisher–Rao Ambiguity Score). Let $p_i \in \Delta^{k-1}$ be the soft assignment vector (e.g., obtained from current centroids via a softmax over squared distances with temperature $T > 0$: $p_i^{(g)} \propto \exp(-\|x_i - \mu_g\|^2/T)$). Let g_1 and g_2 be the two indices with largest probabilities in p_i . Resolve ties in a deterministic way. Define

$$q_i = \left(\frac{p_i^{(g_1)}}{p_i^{(g_1)} + p_i^{(g_2)}}, \frac{p_i^{(g_2)}}{p_i^{(g_1)} + p_i^{(g_2)}} \right), \quad b = \left(\frac{1}{2}, \frac{1}{2} \right).$$

The Fisher–Rao distance is

$$d_{\text{FR}}(q_i, b) = 2 \arccos \left(\frac{1}{\sqrt{2}} (\sqrt{q_{i1}} + \sqrt{q_{i2}}) \right),$$

and the normalized score is

$$J_i = 1 - \frac{2}{\pi} d_{\text{FR}}(q_i, b) \in [0, 1].$$

Definition 5 (Budgeted Information-Geometric Subset). Given a budget m with the feasibility requirement $m \geq |V|$, the optimal subset is $S^* = V \cup \{i_1, \dots, i_{m-|V|}\}$, where the indices i_1, i_2, \dots belong to $\mathcal{S} \setminus V$ and have the largest values of J_i . This construction preserves feasibility since all constraint-violating points remain in V , and the extension outside S^* is fixed as in the previous case.

On S^* we solve the reduced optimization problem of Section 4.1, with the only difference that the working subset is now chosen by the Fisher–Rao scores rather than the margin criterion. Feasibility is again preserved since all violations are contained in V and the external constraints are enforced as before.

Budget Selection Rationale

The budget

$$m = \min \left(\alpha |\mathcal{S}|, |V| + \beta k \log |\mathcal{S}| \right)$$

balances computational constraints with problem complexity. The term $\alpha |\mathcal{S}|$ enforces a hard cap that scales with the dataset size, while the term $|V| + \beta k \log |\mathcal{S}|$ ensures inclusion of all violations plus a logarithmic number of additional ambiguous points per cluster, which captures the effective uncertainty of the problem. Typical choices are $\alpha \in [0.1, 0.3]$ and $\beta \in [2, 5]$.

Proposition 6 (Greedy Optimality under a Modular Objective). Subset S^* maximizes the modular objective $F(S) = \sum_{i \in S} J_i$ subject to $|S| = m$ and $V \subseteq S$. Since F is modular, greedy selection is optimal.

Complexity Computing the two largest entries of each p_i has cost $O(k)$ per point. The total cost to obtain J_i is $O(|\mathcal{S}|k)$. Sorting costs $O(|\mathcal{S}| \log |\mathcal{S}|)$. The overall complexity is $O(|\mathcal{S}|(k + \log |\mathcal{S}|))$, making this approach practical for large-scale clustering problems.

Algorithm 2 Information-Geometric Subset Selection

Require: Soft assignments $\{p_i\}$; violation set V ; budget m with $m \geq |V|$

Ensure: Subset S with $|S| = m$

- 1: $S \leftarrow V$
- 2: Compute J_i for all $i \in \mathcal{S} \setminus V$
- 3: Add to S the $m-|V|$ indices with largest J_i . Break ties in a deterministic way.
- 4: **return** S

Figure 2 illustrates this selection process, showing how ambiguous points and constraint violations are identified and selected. Algorithm 2 provides the complete procedure for information-geometric subset selection.

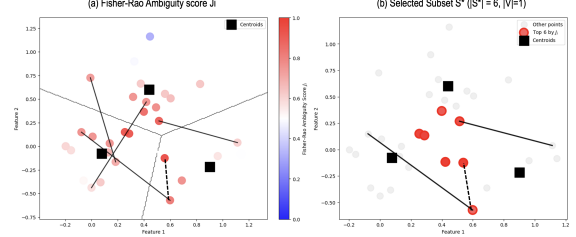


Figure 2: Ambiguity-based subset selection using Fisher-Rao geometry. (a) Fisher-Rao ambiguity scores J_i for each data point (red = ambiguous, blue = certain). Centroids (black squares) and decision boundaries (gray contours) illustrate the clustering structure. Cannot-link constraints are represented by solid black lines, with a constraint violation shown as a dashed black line. (b) Selected subset S^* ($|S^*| = 6, |V| = 1$) including the constraint violation and the most ambiguous points.

5 Pairwise-Aware Subset Selection Framework

We introduce *Pairwise-Aware Subset Selection* (PASS), a k -means framework that scales by concentrating computation on critical regions (Algorithm 3).

Algorithm 3 PASS- k -means framework

Require: data X , clusters k , ML/CL constraints

- 1: **Phase 1: Must-link contraction**
- 2: Collapse must-link components into weighted pseudo-points.
- 3: **Phase 2: Initialization**
- 4: Run mini-batch k -means on contracted data to get initial centroids.
- 5: **Phase 3: Iterative subset refinement**
- 6: **repeat**
- 7: Select subset S with ambiguous or violating points.
- 8: Reassign S via a 0–1 ILP on $\{d_{i,g}\}$ over candidate sets K_i (assignment & CL constraints; feasible local-search fallback).
- 9: Update centroids from new assignments.
- 10: **until** convergence or iteration budget
- 11: **Phase 4: Post-processing**
- 12: Repair residual violations and lift assignments to original data.
- 13: **return** (b, μ)

PASS uses two selectors: **PASS-CA** (margin/violations) and **PASS-IG** (Fisher–Rao uncertainty), with budget $m = \min(\alpha n, |V| + \beta k \log n)$. In each iteration we reassign S by solving a small 0–1 ILP with binaries $d_{i,g}$ for $g \in K_i$ (top- G nearest

Table 1: **Reduction (subset) closes the gap to SOTA:** PASS matches PCCC’s quality on classical pairwise-constrained clustering and scales to 4M+ points (CL, ML, Both; $k = 3$)

Dataset	Method	CL	ML	Both	Dataset	Method	CL	ML	Both
Iris $n = 150$ $d = 4$	COP- k -means	102.03	<u>93.71</u>	86.72	HTRU2 $n = 17,898$ $d = 8$	COP- k -means	No solution found (100 iterations)		
	BLPKM-CC	84.24	<u>83.72</u>	86.83		BLPKM-CC	1.03E+08	<u>1.36E+08</u>	<u>1.44E+08</u>
	PCCC	<u>84.35</u>	<u>83.72</u>	<u>86.75</u>		PCCC	9.21E+07	<u>1.23E+07</u>	<u>1.33E+08</u>
	PASS-CA	84.24	<u>83.72</u>	<u>86.75</u>		PASS-CA	9.35E+07 (13)	1.23E+07	1.32E+08 (13)
	PASS-IG	84.24	<u>83.72</u>	<u>86.75</u>		PASS-IG	<u>9.53E+07</u>	1.23E+07	1.33E+08
Seeds $n = 210$ $d = 7$	COP- k -means	655.55	658.05	656.82	AC $n = 53, 413$ $d = 23$	COP- k -means	No solution found (100 iterations)		
	BLPKM-CC	<u>600.36</u>	<u>629.29</u>	<u>633.91</u>		BLPKM-CC	2.54E+03	<u>2.38E+03</u>	2.60E+03
	PCCC	<u>600.36</u>	627.66	633.25		PCCC	2.24E+03	2.02E+03	2.38E+03
	PASS-CA	<u>600.36</u>	627.66	634.88		PASS-CA	2.25E+03 (9)	2.02E+03	2.51E+03 (20)
	PASS-IG	600.18	<u>627.66</u>	<u>633.91</u>		PASS-IG	2.36E+03	2.02E+03	<u>2.55E+03</u>
Hemi $n = 1,955$ $d = 7$	COP- k -means	1.75E+07	2.44E+07	N/A	Skin $n = 245, 057$ $d = 3$	COP- k -means	No solution found (100 iterations)		
	BLPKM-CC	1.56E+07	2.05E+07	2.36E+07		BLPKM-CC	<u>9.33E+08</u>	<u>1.60E+09</u>	<u>1.63E+09</u>
	PCCC	1.36E+07	1.81E+07	2.10E+07		PCCC	9.30E+08	<u>1.61E+09</u>	1.60E+09
	PASS-CA	1.40E+07 (7)	1.81E+07	2.30E+07 (15)		PASS-CA	8.95E+08 (3523)	1.57E+09	1.57E+09 (4109)
	PASS-IG	1.49E+07	1.81E+07	2.13E+07		PASS-IG	9.30E+08	1.57E+09	1.61E+09 (4)
PR2392 $n = 2,392$ $d = 2$	COP- k -means	N/A		3.68E+10	N/A		Gas_methane $n = 4,178,504$ $d = 18$		
	BLPKM-CC	2.60E+10	<u>3.40E+10</u>	<u>3.77E+10</u>	COP- k -means		No solution found (100 iterations)		
	PCCC	<u>2.77E+10</u>	3.34E+10	3.74E+10	BLPKM-CC		No solution found (1h time limit)		
	PASS-CA	2.58E+10 (4)	3.34E+10	3.82E+10 (10)	PCCC		No solution found (1h time limit)		
	PASS-IG	2.59E+10	3.34E+10	3.86E+10	PASS-CA		No solution found (1h time limit)		
RDS_CNT $n = 10,000$ $d = 3$	COP- k -means	N/A		8.51E+07	N/A		PASS-IG		
	BLPKM-CC	3.00E+07	6.83E+07	8.22E+07	COP- k -means		No solution found (100 iterations)		
	PCCC	2.93E+07	6.23E+07	7.67E+07	BLPKM-CC		No solution found (1h time limit)		
	PASS-CA	2.95E+07 (16)	6.23E+07	7.97E+07 (35)	PCCC		No solution found (1h time limit)		
	PASS-IG	2.98E+07	6.23E+07	8.04E+07	PASS-CA		No solution found (1h time limit)		
Gas_CO $n = 4,208,261$ $d = 18$	COP- k -means	N/A		3.13E+14 (5)	2.67E+14		Gas_CO $n = 4,208,261$ $d = 18$		
	BLPKM-CC	N/A		3.13E+14 (5)	COP- k -means		No solution found (100 iterations)		
	PCCC	N/A		3.13E+14 (5)	BLPKM-CC		No solution found (1h time limit)		
	PASS-CA	N/A		3.13E+14 (5)	PCCC		No solution found (1h time limit)		
	PASS-IG	N/A		3.13E+14 (5)	PASS-IG		No solution found (1h time limit)		

Notes: Parentheses indicate the number of violated constraints. Best per baseline is highlighted in **bold**, second best per baseline is underlined. 1h time limit

centroids, augmented near conflicts), minimizing $\sum_{i \in S} \sum_{g \in K_i} \|x_i - \mu_g\|^2$ subject to $\sum_{g \in K_i} d_{i,g} = 1$, $d_{u,g} + d_{v,g} \leq 1$ for $(u, v) \in \text{CL} \cap (S \times S)$, and forbidding labels that would conflict with outside- S CL partners. We warm-start from current labels and use a deterministic feasible local-search fallback if a MIP solver is unavailable. (The model has $O(mG)$ binaries.) Details are in Appendix B.

Experimental evaluation was conducted on Ubuntu Linux (kernel 6.8.0-51) using a server with an Intel® Xeon® Gold 6230R (104 logical cores, 2.10 GHz) and 187 GiB memory, Gurobi 11.0.2 and Python 3.10.12. Twelve datasets with sample size n and dimensionality d were taken from the UCI Repository (Dua and Graff, 2017). Pairwise constraints follow random-pair sampling as in prior work (Piccialli et al., 2022; Wagstaff et al., 2001; Guns et al., 2016). For each dataset, three scenarios were evaluated: must-link (ML), cannot-link (CL), each with $\frac{n}{4}$ constraints, and Both combines $\frac{n}{4}$ ML and $\frac{n}{4}$ CL. Datasets are grouped as *small* ($n \leq 1,000$), *medium* ($n \leq 10,000$), *large* ($n \leq 100,000$), and *huge* ($n \geq 100,000$).

5.1 Computational Experiments

We report the sum of squared errors (SSE), which is the true MSSC objective computed with the final labels. Note that SSE values are unnormalized and scaled with each dataset, so they are only comparable within the same dataset. We also report the number of violated constraints under ML, CL, and Both

constraints. Runtime and computational performance analysis are provided in the Appendix C. We compare PASS to COP- k -means (Wagstaff et al., 2001) (100 restarts), BLPKM-CC (Baumann, 2020) (exact assignment per iteration), and PCCC (Baumann and Hochbaum, 2024). Best values are put in bold in Table 1.

On small and medium datasets, PASS matches state-of-the-art quality while remaining fast. For well-separated datasets like *Iris*, both PASS variants reach the optimal SSE across all constraint types, indicating that when ambiguity is limited, subset selection preserves the global solution. On *Seeds*, PASS-IG performs best under CL constraints, which is evidence that information-geometric selection resolves boundary cases where cannot-links shift cluster borders while the tie under ML confirms that ML collapsing simplifies the problem without sacrificing quality. **For larger datasets**, PASS maintains competitive performance while enabling scalability not achieved by existing methods. On *AC* and *PR2392*, solutions delivered by PASS-CA are observed to be nearly equivalent to PCCC, particularly under ML constraints where must-link collapsing is demonstrated to be effective. The minimal SSE variations observed under CL and Both constraints are attributed to the inherent challenge of sparse constraint settings rather than methodological limitations. On *Skin*, PASS-CA is found to achieve lower SSE than PCCC, while PASS-IG maintains comparable SSE to PCCC with substantially reduced constraint violations. Most significantly, on the

Gas-methane and *Gas-CO* datasets, only PASS-IG returns solutions, validating its scalability advantages. The logarithmic-sized subset enables feasible optimization where competing methods fail, while maintaining solution quality that approximates state-of-the-art performance. This consistent pattern across dataset sizes provides evidence that PASS delivers both scalability and high-quality solutions, making it suitable for practical applications involving large-scale constrained clustering.

6 Extending to Quantum Clustering

While our classical subset selection framework enables scalability, the reduced problem on the ambiguous subset S remains a challenging combinatorial optimization due to the cannot-link constraints. This core hardness makes it a promising target for quantum heuristics. We therefore extend our framework to quantum clustering to investigate whether near-term quantum devices can effectively solve this extracted, hard subproblem. The connection is natural: pairwise constraints map directly to quadratic couplings in QUBO models, the native input for many quantum optimizers (Cohen et al., 2020; Seong and Park, 2025). However, existing quantum approaches face a fundamental scalability barrier, requiring $O(N \times k)$ variables, which is prohibitive for NISQ devices (Preskill, 2018; Bharti et al., 2022). Our key insight is that **our classical subset selection directly bypasses this barrier**. By identifying the critical subset S , we reduce the quantum variable count to $O(|S| \times k)$, making a resource-aware quantum formulation feasible within hybrid quantum-classical workflows (Harrow, 2020; Tomesh et al., 2020).

6.1 A Quantum Pairwise Constrained Clustering Algorithm

Most NISQ clustering studies focus on unconstrained k -means, leaving the integration of explicit pairwise constraints underexplored in a practical, scalable setting (Cohen et al., 2020). We present a quantum refinement algorithm whose complexity depends on $|S|$, not N . **This allows our method to tackle constrained clustering problems that were previously intractable for near-term quantum hardware, moving beyond small proof-of-concepts.**

Problem (12) is converted to a QUBO by embedding hard constraints as penalties. Let $\lambda = \sum_{i \in S} \sum_{g \in \mathcal{K}} |\Delta_{i,g}| + \varepsilon$, $\varepsilon > 0$, which strictly upper-bounds the variation of the linear term over all assignments; any infeasible configuration incurs at least λ

additional energy (Proposition 12). The penalties are

$$H_{\text{one-hot}} = \lambda \sum_{i \in S} \left(1 - \sum_{g \in \mathcal{K}} d_{i,g} \right)^2, \quad (10a)$$

$$H_{\text{ML}} = \lambda \sum_{(u,v) \in \mathcal{T}_{ml} \cap (S \times S)} \sum_{g \in \mathcal{K}} (d_{u,g} - d_{v,g})^2, \quad (10b)$$

$$H_{\text{CL}} = \lambda \sum_{(u,v) \in \mathcal{T}_{cl} \cap (S \times S)} \sum_{g \in \mathcal{K}} d_{u,g} d_{v,g}. \quad (10c)$$

The full Hamiltonian is

$$\begin{aligned} H(d) &= \sum_{i \in S} \sum_{g \in \mathcal{K}} \Delta_{i,g} d_{i,g} + H_{\text{one-hot}} + H_{\text{ML}} + H_{\text{CL}} + H_{\text{cross}} \\ &= d^\top Q d + c^\top d (+\text{const}). \end{aligned} \quad (11)$$

where H_{cross} groups the linear cross-edge penalties for pairs with exactly one endpoint in S (details in Appendix D.1). A classical re-centering step is followed by quantum refinement on the selected subset S , enforcing one-hot assignment and pairwise constraint feasibility across $|S| \times k$ variables. This formulation constitutes the quantum pairwise constrained clustering algorithm (q-PCKMeans; Appendix D.1).

6.2 Computational Experiments

The evaluation compares qPCKMeans with CP-QAOA (Hadfield et al., 2019), a full encoding of constrained clustering that requires $\mathcal{O}(nk)$ binary variables. This highlights the role of subset selection for quantum clustering: full encodings become impractical on near-term devices due to limited qubits and coherence times. Implementation uses Qiskit 1.3.2 and Python 3.10.12, adhering to the protocol in Section 5. Each circuit employs a single QAOA layer ($p=1$) with 2,048 shots following the few-shot guide of Hao et al. (2024). All runs rely on Qiskit’s `AerSimulator` with IBM-Q noise emulation. We evaluate qPCKMeans on 12 datasets, including 6 UCI datasets (Dua and Graff, 2017) and 6 synthetic. To keep costs tractable while demonstrating scale beyond prior quantum clustering, datasets are capped at $n \leq 900$ and $d \leq 7$. Following Section 5, quality is measured by SSE. Across benchmarks and constraint regimes, q-PCKMeans improves SSE relative to CP-QAOA (reductions of 6–84%) while maintaining competitiveness with classical heuristics. The gains arise from the pairwise-restricted subspace mixer, which prunes infeasible assignments rather than relying on penalties, and from reducing the quantum variable count from $\mathcal{O}(nk)$ to $\mathcal{O}(|S|k)$. Under realistic noise emulation in Appendix D.4, this enables depth-efficient execution up to $n = 900$ while preserving feasibility in reduced space.

Table 2: SSE gains via reduction: solving a reduced (subset) problem, q-PCKMeans achieves lower SSE than full-problem CP-QAOA under CL/ML/Both constraints ($p=1$, shots = 2048)

Real-world datasets						Synthetic datasets ($d = 2$)					
Dataset	Method	CL	ML	Both		Dataset	Method	CL	ML	Both	
Iris $n, d = (150, 4)$ $k = 3$	CP-QAOA	642.78 (26)	678.44 (24)	673.57 (43)		Circles $n = 300$ $k = 2$	CP-QAOA	186.54 (47)	187.93 (36)	187.76 (72)	
	q-PCKMeans (CA)	103.21	109.43 (7)	117.83			q-PCKMeans (CA)	121.92 (22)	119.70 (24)	129.55 (41)	
	q-PCKMeans (IG)	165.48	104.85 (1)	95.87			q-PCKMeans (IG)	150.76	143.38	158.25 (13)	
Seeds $n, d = (210, 7)$ $k = 3$	CP-QAOA	2.67E+03 (30)	2.71E+03 (54)	2.70E+03 (54)		Moons $n = 300$ $k = 2$	CP-QAOA	300.12 (40)	299.30 (24)	296.56 (81)	
	q-PCKMeans (CA)	673.43	674.55	714.85			q-PCKMeans (CA)	152.36	148.49 (12)	152.69	
	q-PCKMeans (IG)	731.02	699.90	730.25			q-PCKMeans (IG)	154.00	153.95	174.06	
Haberman $n, d = (306, 3)$ $k = 2$	CP-QAOA	5.45E+04 (82)	5.45E+04 (33)	5.44E+04 (82)		Spiral $n = 300$ $k = 2$	CP-QAOA	4.10E+03 (36)	4.09E+03 (34)	4.08E+03 (75)	
	q-PCKMeans (CA)	5.11E+04 (25)	5.14E+04 (22)	5.15E+04 (38)			q-PCKMeans (CA)	3.04E+03	2.94E+03	2.66E+03 (37)	
	q-PCKMeans (IG)	5.24E+04 (1)	5.25E+04 (1)	5.28E+04 (14)			q-PCKMeans (IG)	3.08E+03	3.02E+03	3.27E+03 (13)	
Land mine $n, d = (338, 3)$ $k = 5$	CP-QAOA	83.90 (39)	83.30 (50)	83.72 (77)		Moons.2 $n = 400$ $k = 2$	CP-QAOA	798.48 (57)	792.71 (35)	796.21 (81)	
	q-PCKMeans (CA)	26.96	36.64	43.69 (37)			q-PCKMeans (CA)	373.35	368.07	356.25 (20)	
	q-PCKMeans (IG)	27.48	51.11 (9)	50.79 (9)			q-PCKMeans (IG)	381.59	381.98	401.28 (1)	
Monk_2 $n, d = (432, 6)$ $k = 2$	CP-QAOA	1.62E+03 (74)	1.62E+03 (50)	1.62E+03 (117)		An blobs $n = 500$ $k = 3$	CP-QAOA	994.76 (54)	999.75 (53)	997.96 (115)	
	q-PCKMeans (CA)	1.52E+03 (30)	1.52E+03 (26)	1.53E+03 (58)			q-PCKMeans (CA)	153.44	153.44	153.44	
	q-PCKMeans (IG)	1.55E+03	1.55E+03 (1)	1.56E+03 (29)			q-PCKMeans (IG)	154.90	153.94	153.90	
Raisin $n, d = (900, 7)$ $k = 2$	CP-QAOA	2.86E+12 (126)	2.86E+12 (80)	2.86E+12 (66)		Vd blobs $n = 600$ $k = 3$	CP-QAOA	1.20E+03 (70)	1.20E+03 (55)	1.19E+03 (160)	
	q-PCKMeans (CA)	1.45E+12	1.28E+12 (33)	1.29E+12 (49)			q-PCKMeans (CA)	368.67	356.71 (12)	358.01 (19)	
	q-PCKMeans (IG)	1.38E+12	1.49E+12	1.44E+12 (13)			q-PCKMeans (IG)	370.68	410.21 (1)	419.42 (1)	

Notes: Parentheses indicate the number of violated constraints. Best per setting is highlighted in **bold**, 1h time limit.

6.3 Quantum Feasibility and the Path to Advantage

The quantum implementation prioritizes **scalable feasibility over marginal optimality**, a necessary engineering compromise for current NISQ devices. While accepting modest increases in SSE enables execution on existing quantum hardware, the performance gap relative to classical methods primarily reflects current hardware limitations. Our few-shot pipeline (Hao et al., 2024) demonstrates resilience to NISQ-era challenges including shot noise and shallow circuit depths. Critically, this work establishes a theoretical pathway toward future quantum utility. By reducing problems to their ambiguous core—the NP-hard combinatorial kernel that challenges classical solvers—the framework directs quantum resources to computationally valuable subspaces. The logarithmic scaling of the subset size ensures compact QUBOs even for massive datasets, suggesting that future improvements in qubit count and fidelity could enable solving clustering instances that remain challenging for classical exact methods.

7 Conclusion

The paper introduces PASS, a scalable framework for pairwise-constrained k -means that combines must-link collapsing with ambiguity-driven subset selection. By concentrating computation on points with uncertain assignments or constraint violations, PASS maintains competitive solution quality while scaling to million-point datasets where prior methods fail. The reduction also enables initial exploration of quantum-hybrid clustering, suggesting a viable direction for future quantum acceleration.

Limitations Current quantum hardware constraints limit absolute performance and problem scale in our experiments. However, the framework’s logarithmic scaling provides a foundation for potential quantum utility as hardware matures, particularly for the hardest clustering subproblems that challenge classical solvers.

Supplementary Materials for "PASS: Ambiguity Guided Subsets for Scalable Classical and Quantum Constrained Clustering"

This section provides the background, additional proof and further experimental results for our constrained clustering approach. To further support the reproducibility of our results, we will release our experiment code upon acceptance, enabling other researchers to replicate and expand on our work.

A Extended related works

A.1 Quantum Computing Concepts

Classically, the fundamental unit of digital information is the *bit*, definitively holding a value of either 0 or 1. Quantum computation generalizes this notion through the *quantum bit*, or *qubit*, which can exist simultaneously in a coherent superposition of both basis states (Nielsen and Chuang, 2010; Deutsch, 1985). We work in the Noisy Intermediate-Scale Quantum (NISQ) era, characterized by devices with tens to a few hundred qubits that are subject to noise and decoherence; such machines cannot yet support fully fault-tolerant algorithms but may still offer quantum advantage for certain tasks (Preskill, 2018; Arute et al., 2019).

States and Control Primitives Formally, a single qubit lives in the two-dimensional Hilbert space $\mathcal{H}_2 = \text{span}\{|\mathbf{0}\rangle, |\mathbf{1}\rangle\}$, where $|\mathbf{0}\rangle$ and $|\mathbf{1}\rangle$ are the Pauli-Z eigenstates. Any pure state can be written as

$$|\psi\rangle = \alpha|\mathbf{0}\rangle + \beta|\mathbf{1}\rangle, \quad |\alpha|^2 + |\beta|^2 = 1.$$

Geometrically, $|\psi\rangle$ corresponds to a point on the Bloch sphere with polar angles (θ, ϕ) , where $\alpha = \cos(\frac{\theta}{2})$ and $\beta = e^{i\phi} \sin(\frac{\theta}{2})$. Universal gate-based control uses single-qubit rotations

$$R_\alpha(\theta) = \exp(-i\frac{\theta}{2}\sigma_\alpha), \quad \alpha \in \{x, y, z\},$$

and two-qubit entanglers (CNOT) (Barenco et al., 1995). Here σ_α are the Pauli matrices. The *circuit depth* or the number of sequential gate layers serves as a proxy for runtime and accumulated noise on NISQ hardware. In our experiments, we emulate such low-depth circuits with a matrix-product-state (MPS) backend, which compactly represents the limited entanglement produced by shallow QAOA layers.

QUBO to Ising Mapping Many combinatorial problems can be expressed as a Quadratic Unconstrained Binary Optimization (QUBO) problem

$$\min_{z \in \{0,1\}^N} z^\top Q z + c^\top z,$$

where $Q \in \mathbb{R}^{N \times N}$ and $c \in \mathbb{R}^N$. To leverage quantum hardware, we map the binary variables $z_i \in \{0, 1\}$ to Ising spins $s_i \in \{\pm 1\}$ via $s_i = 2z_i - 1$. Under this change of variables the QUBO objective becomes, up to an additive constant, $H_C = \sum_{i < j} J_{ij} Z_i Z_j + \sum_i h_i Z_i$, where Z_i is the Pauli-Z operator on qubit i , and the couplings J_{ij} and fields h_i are algebraically determined by the entries of Q and c . The resulting Hamiltonian H_C encodes the original cost landscape as its diagonal energies, ready for optimization by QAOA.

Quantum Approximate Optimization Algorithm The Quantum Approximate Optimization Algorithm (QAOA) is a hybrid quantum-classical method for approximately solving combinatorial optimization problems by finding the ground state of a diagonal cost Hamiltonian H_C on N qubits (Hilbert-space dimension 2^N ; here $N = |S| \times K$):

$$H_C = \sum_{z \in \{\pm 1\}^N} C(z) |z\rangle\langle z|,$$

where $C(z)$ is the classical objective, such as an Ising-encoded QUBO, and $\{|z\rangle\}$ denotes the computational basis. QAOA constructs a variational state by alternating between the cost and mixer unitaries $U_C(\gamma) = e^{-i\gamma H_C}$, $U_M(\beta) = e^{-i\beta H_M}$, where H_M is a mixer Hamiltonian that induces transitions between computational-basis states. At depth P , the ansatz is

$$|\gamma, \beta\rangle = (U_M(\beta_P) U_C(\gamma_P)) \cdots (U_M(\beta_1) U_C(\gamma_1)) |+\rangle^{\otimes N},$$

with $2P$ variational parameters $\{\gamma_1, \dots, \gamma_P; \beta_1, \dots, \beta_P\}$. A common choice for the mixer is the XY Hamiltonian $H_M = \sum_{i < j} (X_i X_j + Y_i Y_j)$, which preserves Hamming-weight subspaces, thereby enforcing feasibility constraints. The QAOA loop proceeds by (i) preparing $|\gamma, \beta\rangle$, (ii) measuring $\langle H_C \rangle$ on repeated circuit runs, and (iii) updating γ, β via a classical optimizer such as COBYLA to maximise the expected cost. Although theory guarantees monotonic improvement as $P \rightarrow \infty$, in practice small P is chosen on NISQ devices to trade off circuit complexity against approximation quality.

A.2 Extension of constrained clustering with NISQ-friendly QUBO formulation

Quantum computing has attracted interest for clustering, with the goal of obtaining quantum advantage or practical gains in hybrid pipelines Saiphet et al. (2021); Yung and Usman (2024); Chen et al. (2025). Early work casts clustering objectives as Quadratic Unconstrained Binary Optimization (QUBO) problems and solves them on quantum annealers Zaiou et al. (2021) or with gate based QAOA, establishing feasibility (Boros et al., 2007). These approaches are limited by nonconvex energy landscapes, which benefit from careful warm starts or mixer design, and by the quadratic growth of one hot QUBO encodings, which strains qubit counts and coherence times Kumari and Ghose (2018); Tomesh et al. (2021b); Egger et al. (2021); Mirkarimi et al. (2024b). To improve scaling, some methods compress the dataset before forming QUBOs; for instance, qc-kmeans builds a constant size sketch and then solves small QUBOs with shallow QAOA (Chumpitaz-Flores et al., 2025b). Empirical studies therefore remain focused on small datasets or reduced coresets, with accuracy that often matches or trails classical baselines. Despite progress in quantum clustering without constraints, only a few annealer based proofs of concept address constrained clustering Cohen et al. (2020); Richoux et al. (2023); Seong and Park (2025). These works do not provide a systematic treatment of pairwise constraints, leaving this setting largely open.

B 0–1 ILP for Phase 3

Let $S \subseteq \{1, \dots, n\}$ be the working subset and $\{\mu_g\}_{g=1}^k$ be the current set of centroids. For each $i \in S$, let $K_i \subseteq \{1, \dots, k\}$ be the candidate cluster set and introduce binary variables $d_{i,g} \in \{0, 1\}$ for $g \in K_i$, indicating assignment of i to g . Let g_i^{cur} denote the current label and $c_i^{\text{cur}} = \|x_i - \mu_{g_i^{\text{cur}}}\|^2$. Define the incremental cost

$$\Delta_{i,g} = \|x_i - \mu_g\|^2 - c_i^{\text{cur}}, \quad g \in K_i.$$

By construction, if $g_i^{\text{cur}} \in K_i$ then $\Delta_{i,g_i^{\text{cur}}} = 0$. Because we enforce $\sum_{g \in K_i} d_{i,g} = 1$ (below), $\sum_{i \in S} c_i^{\text{cur}}$ is constant and Phase 3 minimizes the restricted SSE via the linear objective

$$\min_d \sum_{i \in S} \sum_{g \in K_i} \Delta_{i,g} d_{i,g}.$$

B.1 Feasibility Constraints

One-hot assignment: each $i \in S$ selects exactly one cluster

$$\sum_{g \in K_i} d_{i,g} = 1, \quad \forall i \in S.$$

Cannot-link within S : for any $(u, v) \in \mathcal{T}_{\text{cl}}$ with $u, v \in S$,

$$d_{u,g} + d_{v,g} \leq 1, \quad \forall g \in K_u \cap K_v.$$

Cross- S consistency: for $(u, v) \in \mathcal{T}_{\text{cl}}$ with $u \in S$ and $v \notin S$, letting $g^*(v)$ be the fixed label of v , forbid u from taking $g^*(v)$ by clamping

$$d_{u,g^*(v)} = 0,$$

i.e., an upper-bound 0 on the corresponding binary variable.

B.2 Implementation Details

Candidate sets. For $i \in S$, initialize K_i with the nearest G centroids to x_i (default $G=4$); if i is a CL violator under the current assignment or adjacent (in the CL graph) to a violator, set $K_i \leftarrow \{1, \dots, k\}$; otherwise augment K_i with the current label of i and the current labels of its CL neighbors.

Warm start and time limit. If $g_i^{\text{cur}} \in K_i$, set $d_{i,g_i^{\text{cur}}} \leftarrow 1$ as a MIP start; solve under a wall-clock time limit. If a MILP solver is unavailable, use a deterministic feasible local-search fallback.

Algorithm 4 Phase 3: Restricted 0–1 ILP on S

Require: Data X , centers $\{\mu_g\}$, current labels $\{g_i^{\text{cur}}\}$, subset S , CL set \mathcal{T}_{cl} , parameter G

- 1: Build CL adjacency; mark violators $\mathcal{V} = \{i : \exists(i, j) \in \mathcal{T}_{\text{cl}}, g_i^{\text{cur}} = g_j^{\text{cur}}\}$
- 2: **for** $i \in S$ **do**
- 3: $K_i \leftarrow$ top- G nearest centroids to x_i
- 4: **if** $i \in \mathcal{V}$ **or** i is adjacent to \mathcal{V} **then**
- 5: $K_i \leftarrow \{1, \dots, k\}$
- 6: **end if**
- 7: $K_i \leftarrow K_i \cup \{g_i^{\text{cur}}\} \cup \{g_j^{\text{cur}} : (i, j) \in \mathcal{T}_{\text{cl}}\}$
- 8: **end for**
- 9: For $i \in S$, set $c_i^{\text{cur}} = \|x_i - \mu_{g_i^{\text{cur}}}\|^2$ and $\Delta_{i,g} = \|x_i - \mu_g\|^2 - c_i^{\text{cur}}$ for $g \in K_i$
- 10: Create binaries $d_{i,g}$ for $i \in S, g \in K_i$
- 11: Add constraints: (i) $\sum_{g \in K_i} d_{i,g} = 1$; (ii) $d_{u,g} + d_{v,g} \leq 1$ for $(u, v) \in \mathcal{T}_{\text{cl}}$ with $u, v \in S$ and $g \in K_u \cap K_v$; (iii) set $\text{UB}(d_{u,g^*(v)}) = 0$ for $(u, v) \in \mathcal{T}_{\text{cl}}$ with $u \in S, v \notin S$
- 12: Set objective $\min \sum_{i \in S} \sum_{g \in K_i} \Delta_{i,g} d_{i,g}$
- 13: Warm start: if $g_i^{\text{cur}} \in K_i$ then set $d_{i,g_i^{\text{cur}}} \leftarrow 1$; solve with time limit; decode $\hat{g}_i \leftarrow \arg \max_{g \in K_i} d_{i,g}$ for $i \in S$

Size and complexity. The model has $\sum_{i \in S} |K_i|$ binaries, thus $O(|S|G)$ under normal operation, rising to $O(|S|k)$ only for nodes in or adjacent to CL violations due to candidate expansion. Constraints include $|S|$ one-hot equalities; at most

$$\sum_{(u,v) \in \mathcal{T}_{\text{cl}} \cap (S \times S)} |K_u \cap K_v|$$

CL inequalities (added only when $K_u \cap K_v \neq \emptyset$); and a linear number of cross- S clamps from \mathcal{T}_{cl} .

C Runtime and Computational Performance

C.1 Phase-Wise Cost Breakdown

The per iteration wall clock time splits into three phases: subset selection, restricted zero-one integer linear program reassignment, and centroid recomputation. Across datasets under BOTH with IG, the integer linear program phase accounts for the largest share on average, while selection and centroid updates contribute comparable shares as reported in Table 3. The shares vary with dataset size. In **iris** and **seeds** the integer linear program share is higher. In **skin**, the selection and centroid phases take a larger portion of the iteration time.

This pattern follows two empirical observations. First, the integer linear program problem size per iteration, measured by the maximum number of binary variables, grows with n as shown in Figure 4. Second, the integer linear program is restricted to an active subset whose average fraction of n decreases as n grows. In **skin** the active subset is below one percent of n . In **iris** and **seeds** it is near one sixth. Thus the absolute number of integer linear program variables increases with n , while the share of time in the integer linear program decreases in the largest dataset. Subset selection and centroid updates process the full dataset in each iteration, so their shares rise in **skin**.

The three instrumented phases account for most of the accumulated time. The remaining share corresponds to orchestration and utilities such as data structures, input output, and logging. This explains why the three columns in the table do not sum to one. Implications. For small and medium instances, prioritize improvements in the integer linear program phase. As n increases, focus also on subset selection and centroid updates using sampling schemes, neighborhood data structures, or partial updates.

Dataset	n	Selection	ILP	Centroids	Max Binaries
iris	150	12.6%	68.4%	8.5%	56
seeds	210	10.9%	71.7%	7.6%	125
hemi	1,955	15.4%	57.8%	13.7%	1,441
pr2392	2,392	16.3%	56.3%	14.8%	1,574
AC_FL	7,195	16.4%	58.8%	15.3%	4,756
rds_cnt	10,000	17.3%	56.2%	17.1%	6,647
HTRU2_L	17,898	18.4%	51.1%	17.8%	10,635
skin	245,057	35.0%	25.6%	25.9%	49,507

Table 3: Phase-wise time shares (sum over iterations) and maximum number of binaries per iteration for IG under BOTH.

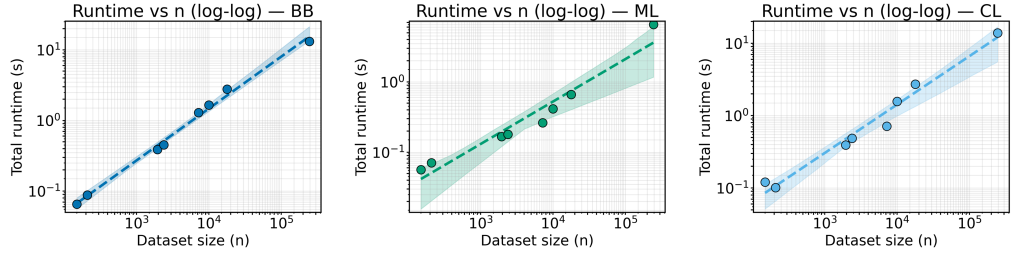


Figure 3: Total runtime vs. n (log–log) shows near-linear scaling. Runtime grows $\sim 201\times$ for a $1,633\times$ dataset size increase.

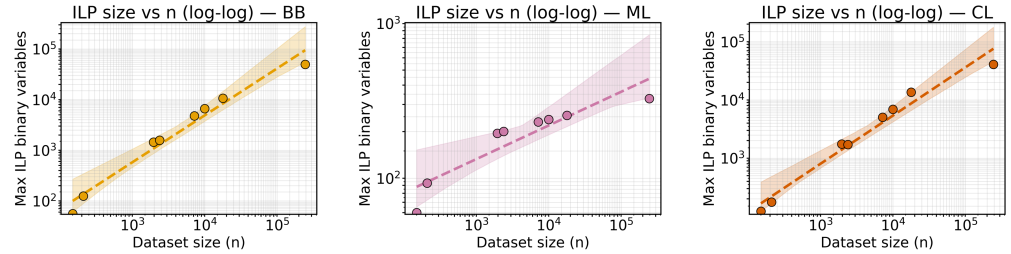


Figure 4: Maximum ILP binaries vs. n (log–log). Across the range, the maximum binaries increase $\sim 884\times$.

C.2 Time and Memory Scaling with Problem Size

Total runtime, computed as the sum over per iteration times, follows a power law with respect to n as shown in Figure 3, with coefficient of determination $R^2 = 0.994$. From **iris**, where $n = 150$, to **skin**, where $n = 245,057$, runtime increases from 0.065 seconds to 13.179 seconds, which is a factor of two hundred for a factor of one thousand six hundred in dataset size. The maximum number of binary variables in the integer linear program per iteration also grows with n and fits a power law with coefficient of determination $R^2 = 0.969$. Across the same endpoints this count increases by a factor of eight hundred eighty four, as shown in Figure 4.

These trends match the phase wise breakdown. The zero–one integer linear program runs on an active subset whose average fraction of n decreases as n grows. In **skin** the active subset is below one percent of n , while in **iris** and **seeds** it is near one sixth. Hence the absolute problem size of the integer linear program increases with n , while its share of iteration time decreases in the largest instance. Subset selection and centroid updates operate on all points in each iteration, so their shares increase with n . As a result the total runtime grows more slowly than n while the memory proxy tracks n more closely.

C.3 Convergence and Constraint Satisfaction

We define stabilization as the first iteration with zero violations and a relative change in the sum of squared errors below 10^{-3} . Across datasets, stabilization occurs within one to nine iterations, with an average of 3.6. We do not observe a clear monotonic relation between dataset size and iterations to stabilization.

Final feasibility meets the target in `iris`, `seeds`, `hemi`, `pr2392`, and `HTRU2_L`, which end with zero violations. The remaining datasets report violation rates of 0.28 percent for `rds_cnt`, 0.17 percent for `AC_FL`, and 0.0065 percent for `skin`. These rates are below one half of one percent of the corresponding cannot link constraints and below one percent of all pairwise constraints. The iteration traces show that once the integer linear program resolves conflicts on the active subset and centroid changes are small, the procedure reaches a state with no violations or a small residual set relative to the total number of constraints.

D q-PCKMeans: A Quantum Pairwise Constrained Clustering Algorithm

D.1 Quantum Variational Framework

QUBO formulation To enable scalable quantum optimization, we restrict the problem to a subset $S \subseteq \mathcal{S}$ of ambiguous or constraint-violating samples, with $|S| \ll |\mathcal{S}|$, and formulate the following reduced Quadratic Unconstrained Binary Optimization:

$$\min_d \quad \sum_{i \in S} \sum_{g \in \mathcal{K}} \Delta_{i,g} d_{i,g} \quad (12a)$$

$$\text{s.t.} \quad \sum_{g \in \mathcal{K}} d_{i,g} = 1, \quad \forall i \in S, \quad (12b)$$

$$d_{u,g} = d_{v,g}, \quad \forall (u, v) \in \mathcal{T}_{ml} \cap (S \times S), \forall g \in \mathcal{K}, \quad (12c)$$

$$d_{u,g} + d_{v,g} \leq 1, \quad \forall (u, v) \in \mathcal{T}_{cl} \cap (S \times S), \forall g \in \mathcal{K}, \quad (12d)$$

$$d_{i,g} \in \{0, 1\}, \quad \forall i \in S, g \in \mathcal{K}. \quad (12e)$$

For edges with one endpoint in S and the other in $\mathcal{S} \setminus S$, we add linear penalties that forbid assigning the in- S endpoint to the fixed label of its partner, mirroring the reduced classical formulation. Concretely, for $(u, v) \in \mathcal{T}_{cl}$ with $u \in S, v \notin S$ and fixed label $g^*(v)$, we add $\lambda d_{u,g^*(v)}$; for $(u, v) \in \mathcal{T}_{ml}$ with $u \in S, v \notin S$, we add the linear terms

$$\lambda \sum_{g \in \mathcal{K}} d_{u,g} - 2\lambda d_{u,g^*(v)},$$

which, under the one-hot constraint $\sum_g d_{u,g} = 1$, are equivalent (up to an additive constant that does not affect the optimum) to the penalty $\lambda(1 - 2d_{u,g^*(v)})$ that encourages u to match $g^*(v)$. The symmetric cases with $v \in S, u \notin S$ are handled analogously.

The coefficients $\Delta_{i,g}$ capture the incremental sum of squared errors: $\Delta_{i,g} = \|x_i - \mu_g\|^2 - \|x_i - \mu_{g^*(i)}\|^2$, where $g^*(i)$ denotes the current cluster assignment of sample i . The binary decision variable $d_{i,g} = 1$ indicates reassigning i to cluster g .

Problem (12) can be converted to a QUBO suitable for quantum optimization by embedding the hard constraints as penalty terms in the Hamiltonian. Let $\lambda = \sum_{i \in S} \sum_{g \in \mathcal{K}} |\Delta_{i,g}| + \varepsilon$, $\varepsilon > 0$, which is strictly larger than the maximum possible variation of the linear cost over all assignments. Any infeasible solution therefore incurs an energy penalty of at least λ , guaranteeing it ranks above every feasible configuration, as shown in Proposition 12. With this choice of λ , one-hot, must-link, and cannot-link constraints translate into the following quadratic penalties:

$$H_{\text{one-hot}} = \lambda \sum_{i \in S} \left(1 - \sum_{g \in \mathcal{K}} d_{i,g} \right)^2, \quad (13a)$$

$$H_{\text{ML}} = \lambda \sum_{(u,v) \in \mathcal{T}_{ml} \cap (S \times S)} \sum_{g \in \mathcal{K}} (d_{u,g} - d_{v,g})^2, \quad (13b)$$

$$H_{\text{CL}} = \lambda \sum_{(u,v) \in \mathcal{T}_{cl} \cap (S \times S)} \sum_{g \in \mathcal{K}} d_{u,g} d_{v,g}. \quad (13c)$$

The full QUBO Hamiltonian is

$$H(d) = \sum_{i \in S} \sum_{g \in \mathcal{K}} \Delta_{i,g} d_{i,g} + H_{\text{one-hot}} + H_{\text{ML}} + H_{\text{CL}} + H_{\text{cross}}, \quad (14)$$

where H_{cross} collects the linear cross-edge penalties described above. Up to an additive constant, the Hamiltonian can be written in matrix form as $H(d) = d^\top Q d + c^\top d$. This formulation yields $n_{\text{qubo}} = |S| \times k$ binary variables and embeds all hard constraints directly into the QUBO. We construct a QAOA ansatz with a one-hot preserving mixer that is invariant on the subspace defined by $\sum_g d_{i,g} = 1$ for each i , so that the one-hot penalty remains inactive during the variational evolution. Leveraging this invariant subspace, we derive an additive improvement bound for depth $p = 1$ on the expected performance of the algorithm.

We introduce a variational algorithm that operates on a reduced subspace of ambiguous samples while enforcing hard constraints. The framework has three parts: a one-hot preserving mixer that restricts evolution to the feasible one-hot subspace; an additive improvement bound that applies at depth $p = 1$; and a warm-start depth reduction showing how a classical seed reduces circuit depth in practice.

One-Hot Preserving Mixer To guarantee that the one-hot constraint remains satisfied throughout the variational evolution, we employ a point-wise XY mixer that acts within the one-hot subspace. Must-link and cannot-link constraints are enforced via the penalty Hamiltonian described in Section D.1. Although intermediate QAOA superpositions can carry amplitude on must-link and cannot-link violating basis states, the penalty terms shift those states upward in energy according to λ . Throughout, let X , Y , and Z denote the single-qubit Pauli matrices:

$$X = \begin{pmatrix} 0 & 1 \\ 1 & 0 \end{pmatrix}, \quad Y = \begin{pmatrix} 0 & -i \\ i & 0 \end{pmatrix}, \quad Z = \begin{pmatrix} 1 & 0 \\ 0 & -1 \end{pmatrix}.$$

For a qubit indexed by $\ell(i, g) = k(i-1) + g$, we write $X_{i,g}$ for X acting on that qubit, and likewise $Y_{i,g}$ and $Z_{i,g}$. *Definition 7* (Point-wise XY Mixer). For each ambiguous sample $i \in S$ and each unordered pair of clusters (g, h) with $g < h$, define the two-qubit unitary $U_{i,(g,h)}(\beta) = \exp(-i\beta [X_{i,g}X_{i,h} + Y_{i,g}Y_{i,h}])$, where $X_{i,g}, Y_{i,g}$ act on qubit $\ell(i, g) = k(i-1) + g$. The global mixer is the product $U_M(\beta) = \prod_{i \in S} \prod_{g < h} U_{i,(g,h)}(\beta)$.

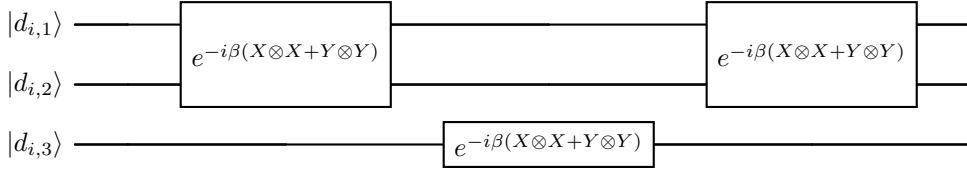


Figure 5: One-hot preserving mixer for $k = 3$: apply the three two-qubit blocks $e^{-i\beta(X_{i,g}X_{i,h} + Y_{i,g}Y_{i,h})}$ for the pairs $(g, h) = (1, 2), (1, 3), (2, 3)$. No single-qubit R_X rotations are used.

Lemma 8 (Invariance of the One-Hot Subspace). Let $\mathcal{H}_{\text{one-hot}} = \text{Span}\{|d\rangle : \sum_{g=1}^k d_{i,g} = 1, \forall i \in S\}$. Then, for all β , $U_M(\beta) \mathcal{H}_{\text{one-hot}} \subseteq \mathcal{H}_{\text{one-hot}}$.

Proof. Fix a sample i and define the population operator $N_i = \sum_{g=1}^k \frac{1-Z_{i,g}}{2}$, whose eigenvalue on a computational basis state is the Hamming weight $\sum_g d_{i,g}$. A state $|\psi\rangle$ satisfies the one-hot constraint if and only if $N_i |\psi\rangle = |\psi\rangle$. Using the commutation relations $[X, Z] = 2iY$ and $[Y, Z] = -2iX$, one checks $[N_i, X_{i,g}X_{i,h} + Y_{i,g}Y_{i,h}] = 0$ for all $g < h$. Hence each local mixer $U_{i,(g,h)}(\beta)$ commutes with N_i , and so does the global $U_M(\beta)$. Therefore $U_M(\beta)$ preserves the eigenspace $N_i = 1$ for every i , and hence preserves $\mathcal{H}_{\text{one-hot}}$. \square

Remark 9. The mixer preserves one-hot but does not enforce must-link or cannot-link relations. Any intermediate state that violates these relations remains in the computational basis yet incurs an energy penalty of at least $\lambda > \sum_{i,g} |\Delta_{i,g}|$ as in Proposition 12.

Lemma 10 (Gate Count and Circuit Depth). Implementing $U_M(\beta)$ uses $\binom{k}{2}$ logical $XX+YY$ blocks per sample $i \in S$, for a total of $|S| \binom{k}{2} = O(k^2|S|)$ blocks. Prior to hardware transpilation, the circuit depth is $O(k)$ per sample and remains $O(k)$ overall, since all samples can be processed in parallel.

Proof. For each sample i and each pair $g < h$, the unitary $\exp[-i\beta(X_{i,g}X_{i,h} + Y_{i,g}Y_{i,h})]$ is one $XX+YY$ block. There are $\binom{k}{2}$ such pairs, so the total count is $|S|\binom{k}{2} = O(k^2|S|)$. To bound the depth for a fixed i , view these pairs as edges of the complete graph K_k . When k is even, K_k decomposes into $k-1$ perfect matchings; when k is odd, its edge-chromatic number is k , yielding k matchings each acting on disjoint qubit pairs. Thus the mixer uses $k-1$ layers if k is even and k layers if k is odd, which is $O(k)$. Each $XX+YY$ block further expands into a constant-size native pattern, which does not change the asymptotic depth. Since different samples act on disjoint registers, all sample mixers can run in parallel, preserving the $O(k)$ overall depth. \square

Native gate accounting. In a native two-qubit gate set with RXX and RYY , each logical $XX+YY$ block maps to two native two-qubit gates per pair, for a total of $2\binom{k}{2}$ native two-qubit gates per sample.

Corollary 11 (Depth on Linear Connectivity). When the hardware graph is a linear nearest-neighbour chain, the edges of K_k require an additional routing step; one schedule yields depth $O(k^2)$ per sample and $O(k^2)$ overall, still independent of $|S|$ due to inter-sample parallelism.

Proposition 12 (Penalty Weight Sufficiency). Let $\lambda > \sum_{i \in S} \sum_{g=1}^k |\Delta_{i,g}|$. Then any assignment that violates at least one constraint in Eqs. (12b)–(12d) has energy strictly larger than any feasible assignment.

Proof. Each violated constraint contributes at least λ to the Hamiltonian in Eq. (14), while the linear cost term can differ by at most $\sum_{i,g} |\Delta_{i,g}|$. Therefore any infeasible assignment incurs a net energy penalty exceeding that bound. \square

Penalty scale The lower bound on λ that separates feasible from infeasible assignments can conflict with upper ranges that yield a nonzero depth $p = 1$ improvement bound. The additive improvement bound in Theorem 14 applies when $\lambda \leq \bar{\eta}|S|/(2\kappa)$. In practice, a schedule for λ can be used: moderate values during the variational search and larger values for final evaluation that enforce feasibility separation. In particular, during the search phase we choose

$$\lambda \leq \lambda_{\text{limit}} := \frac{\bar{\eta}|S|}{32(k-1)(|\mathcal{E}_{\text{ML}}| + |\mathcal{E}_{\text{CL}}|)},$$

with $\mathcal{E}_{\text{ML}} := \mathcal{T}_{ml} \cap (S \times S)$ and $\mathcal{E}_{\text{CL}} := \mathcal{T}_{cl} \cap (S \times S)$, and then increase λ at evaluation time to enforce feasibility separation.

For the running example with $|S| = 6$ and $k = 3$, the QUBO in Eq. (12) uses $n_{\text{qubo}} = k|S| = 18$ binary variables. Choosing $\lambda > \sum_{i \in S} \sum_g |\Delta_{i,g}|$ ensures any constraint violation incurs a penalty above any cost improvement. The one-hot mixer in Definition D.1 and Lemma 8 applies three two-qubit $XX+YY$ blocks per sample, and on a linear connectivity graph the routing schedule of Corollary 11 achieves depth $O(k^2) = 9$ per sample, independent of $|S|$.

D.2 Additive Improvement Theorem ($p = 1$)

We analyze a single-layer $p = 1$ QAOA ansatz under a global budget of $\mathcal{O}(10^3)$ measurement shots. In this setting, the computational cost depends on the cardinality of the ambiguous set S . We capture the remaining improvement potential via the average ambiguity margin $\bar{\eta}$, which dictates the additive gain from one QAOA layer.

Definition 13 (Incremental cost and ambiguity margin). Let $g^*(i)$ denote the current cluster of sample i with respect to the present centroids $\{\mu_g\}_{g=1}^k$. For $i \in S$ define the point-wise margin $\eta_i = \max\{0, \min_{g \neq g^*(i)} (\|x_i - \mu_{g^*(i)}\|^2 - \|x_i - \mu_g\|^2)\}$. Thus $\eta_i > 0$ if and only if at least one alternative cluster shortens the distance of x_i to its centroid. The average ambiguity margin is $\bar{\eta} = \frac{1}{|S|} \sum_{i \in S} \eta_i$.

QUBO cost Given $\Delta_{i,g} = \|x_i - \mu_g\|^2 - \|x_i - \mu_{g^*(i)}\|^2$, let $f(z) = \sum_{i \in S} \sum_{g=1}^k \Delta_{i,g} z_{i,g}$. For the feasible bit-string $d^{(0)}$ produced by the classical pre-solver, one has $H(d^{(0)}) = f(d^{(0)})$, as all one-hot, must-link, and cannot-link constraints are satisfied, nullifying penalty terms.

Theorem 14 (Additive improvement with one layer $p = 1$ under penalties). Let $|d^{(0)}\rangle \in \mathcal{H}_{\text{one-hot}}$ be a feasible state and decompose the Hamiltonian as $H = f(\hat{d}) + H_{\text{pen}}$, where $H_{\text{pen}} = H_{\text{one-hot}} + H_{\text{ML}} + H_{\text{CL}}$. Let $B =$

$\sum_{i \in S} \sum_{g < h} (X_{i,g} X_{i,h} + Y_{i,g} Y_{i,h})$ be the one-hot preserving mixer from Lemma 8. Choose $\beta = c/\sqrt{|S|}$ with $0 < c \leq \pi/6$, and define $|\psi_1\rangle = U_M(\beta) U_C(\gamma) |d^{(0)}\rangle$, with $U_M(\beta) = e^{-i\beta B}$ and $U_C(\gamma) = e^{-i\gamma H}$. Then

$$\langle \psi_1 | H | \psi_1 \rangle = f(d^{(0)}) - (\bar{\eta} |S| - \kappa \lambda) \beta^2 + \mathcal{O}(\beta^3),$$

where $\kappa := 16(k-1)(|\mathcal{E}_{\text{ML}}| + |\mathcal{E}_{\text{CL}}|)$, with $\mathcal{E}_{\text{ML}} := \mathcal{T}_{\text{ml}} \cap (S \times S)$ and $\mathcal{E}_{\text{CL}} := \mathcal{T}_{\text{cl}} \cap (S \times S)$. Moreover, if $\lambda \leq \frac{\bar{\eta} |S|}{2\kappa}$, then

$$\langle \psi_1 | H | \psi_1 \rangle \leq f(d^{(0)}) - \frac{1}{2} c^2 \bar{\eta} + \mathcal{O}(|S|^{-1/2}),$$

which yields an additive improvement proportional to $\bar{\eta}$.

Proof. Since $U_C(\gamma) = e^{-i\gamma H}$ is diagonal and $|d^{(0)}\rangle$ is an eigenstate of H , it contributes only a global phase, so $\langle \psi_1 | H | \psi_1 \rangle = \langle d^{(0)} | U_M^\dagger(\beta) H U_M(\beta) | d^{(0)} \rangle$. The one-hot penalty $H_{\text{one-hot}}$ annihilates $|d^{(0)}\rangle$ and $U_M(\beta)$ preserves $H_{\text{one-hot}}$, so its contribution vanishes. Using the Baker–Campbell–Hausdorff expansion, $U_M^\dagger H U_M = H + i\beta[B, H] + \frac{\beta^2}{2}[B, [B, H]] + \mathcal{O}(\beta^3)$. Because H is diagonal and B flips two bits, $\langle d^{(0)} | [B, H] | d^{(0)} \rangle = 0$. Taking expectations,

$$\langle \psi_1 | H | \psi_1 \rangle = f(d^{(0)}) + \frac{\beta^2}{2} \langle d^{(0)} | [B, [B, f]] | d^{(0)} \rangle + \frac{\beta^2}{2} \langle d^{(0)} | [B, [B, H_{\text{pen}}]] | d^{(0)} \rangle + \mathcal{O}(\beta^3).$$

From the analysis of the linear term, $[B, [B, f]] = -2 \sum_{i \in S} \eta_i$, giving the term $-\bar{\eta} |S| \beta^2$. For each must-link or cannot-link edge, a nested-commutator norm bound $\|[B, [B, \cdot]]\| \leq 16(k-1)$ holds; summing over $|\mathcal{E}_{\text{ML}}| + |\mathcal{E}_{\text{CL}}|$ edges yields $\frac{\beta^2}{2} \langle d^{(0)} | [B, [B, H_{\text{pen}}]] | d^{(0)} \rangle \leq \kappa \lambda \beta^2$. Combining these bounds gives the claim. If $\lambda \leq \bar{\eta} |S|/(2\kappa)$ the coefficient of β^2 is at most $-\frac{1}{2} \bar{\eta}$; with $\beta = c/\sqrt{|S|}$ the remainder scales as $\mathcal{O}(|S|^{-1/2})$, completing the proof. \square

D.3 Comparison with Classical Heuristic Algorithms

We evaluate two variants of *q-PCKMeans* against three widely used constrained-clustering heuristics: COP-KMeans (Wagstaff et al., 2001), MPCKMeans (Bilenko et al., 2004), and PCKMeans (Basu et al., 2004). Table 4 (*Performance of classical clustering heuristics with constraints*) reports the sum of squared errors (SSE) together with the fraction of violated constraints (shown in parentheses) in three constraint cases, namely must-link only (ML-only), cannot-link only (CL-only), and both (Both) for each dataset and constraint regime.

Across datasets, the classical heuristics exhibit the expected trade-off between clustering distortion and constraint satisfaction: PCKMeans/MPCKMeans often reach lower SSE on some instances but at the cost of nonzero violation rates, whereas COP-KMeans enforces constraints when it returns a solution, yet can fail to converge or produce a feasible assignment in certain regimes. By contrast, *q-PCKMeans* satisfies all given constraints in our experiments while remaining competitive in SSE, matching or improving upon the heuristics on many datasets despite optimizing over a reduced subset.

To our knowledge, there are no published quantum methods that directly address pairwise-constrained k -means; existing NISQ studies focus on unconstrained k -means. We therefore benchmark against the standard classical heuristics under identical inputs and constraint regimes. We omit exact ILP solvers and specialized meta-heuristics because they target materially different formulations and entail unequal computational assumptions relative to the NISQ-oriented setting considered here.

D.4 Clustering evaluation

Our study distinguishes two components of clustering performance: (i) the formulation, which determines the approach to measuring data similarity and influences metrics such as ARI, AMI, and purity; and (ii) the solution quality, assessed by cost minimization. We emphasize the solution quality specifically for the K-Means cost. To further analyze this, we conducted additional statistical evaluations and present ARI, AMI, and purity scores obtained from six datasets with available ground truth labels, comparing our results against the algorithm proposed by Lloyd (1982); McQueen (1967), as summarized in Table 5. In all experiments, the number of clusters matches the count of ground truth labels.

Table 4: Performance of classical clustering heuristics with constraints.

Dataset	Method	Cannot-link			Must-link			Both-link		
		SSE	Runtime (s)	Violation Rate	SSE	Runtime (s)	Violation Rate	SSE	Runtime (s)	Violation Rate
Iris N=150 m = 4 k=3	cop-kmeans	157.75	0.0785	0.0000	155.30	0.6251	0.0000	108.93	1.3485	0.0000
	mpckmeans	114.21	0.0587	0.0013	180.98	0.0380	0.0080	156.31	0.0863	0.0149
	pckmeans	118.60	0.0282	0.0040	155.47	0.0208	0.0187	120.47	0.0308	0.0054
	q-PCKMeans (CA)	103.21	33.6785	0.0000	109.43	44.2633	0.1400	117.83	34.0471	0.0000
	q-PCKMeans (IG)	165.48	49.9614	0.0000	104.85	59.1639	0.0133	95.87	49.4490	0.0000
Seeds N=210 m = 7 k=3	cop-kmeans	887.30	1.2976	0.0000	No solution found			No solution found		
	mpckmeans	705.93	0.0823	0.0000	1092.12	0.0689	0.0152	888.79	0.2333	0.0010
	pckmeans	855.49	0.0479	0.0000	1011.51	0.0340	0.0162	964.02	0.0355	0.0163
	q-PCKMeans (CA)	673.43	43.2233	0.0000	674.55	38.2600	0.0000	714.85	45.1886	0.0000
	q-PCKMeans (IG)	731.02	62.6145	0.0000	699.90	65.2015	0.0000	730.25	62.0752	0.0000
Circles n = 300 m = 2 k=2	cop-kmeans	No solution found			No solution found			No solution found		
	mpckmeans	126.56	0.2084	0.3527	163.37	0.1229	0.0447	158.47	1.0551	0.0513
	pckmeans	162.63	0.0504	0.0613	160.88	0.0366	0.0540	156.73	0.0398	0.0607
	q-PCKMeans (CA)	121.92	71.5198	0.2978	119.70	48.8111	0.3244	129.55	110.1190	0.2778
	q-PCKMeans (IG)	150.76	44.3893	0.0000	143.38	39.4976	0.0000	158.25	94.5453	0.0844
Moons n = 300 m = 2 k=2	cop-kmeans	No solution found			No solution found			No solution found		
	mpckmeans	142.46	0.1440	0.1027	198.77	0.0892	0.0147	213.69	1.3652	0.0300
	pckmeans	178.04	0.0667	0.0427	180.76	0.0353	0.0340	189.02	0.0484	0.0433
	q-PCKMeans (CA)	152.36	30.7984	0.0000	148.49	34.8021	0.0000	152.69	54.8566	0.0800
	q-PCKMeans (IG)	154.00	32.9176	0.0000	153.95	32.5103	0.0000	174.06	49.4564	0.0000
Spiral n = 300 m = 2 k=2	cop-kmeans	No solution found			No solution found			No solution found		
	mpckmeans	2.82E+03	0.1835	0.2807	3.73E+03	0.1365	0.0353	3.71E+03	0.9405	0.0467
	pckmeans	3.60E+03	0.0519	0.0600	3.67E+03	0.0485	0.0433	3.54E+03	0.0418	0.0433
	q-PCKMeans (CA)	3.04E+03	34.4628	0.0000	2.94E+03	41.0780	0.0000	2.66E+03	129.7194	0.2444
	q-PCKMeans (IG)	3.08E+03	36.7940	0.0000	3.02E+03	34.3830	0.0000	3.27E+03	94.7219	0.0844
Haberman n = 306 d = 3 k=2	cop-kmeans	No solution found			No solution found			No solution found		
	mpckmeans	5.18E+04	0.1279	0.2288	5.15E+04	0.0969	0.0588	5.02E+04	0.6596	0.0539
	pckmeans	5.04E+04	0.0593	0.0510	5.07E+04	0.0425	0.0725	5.04E+04	0.0400	0.0605
	q-PCKMeans (CA)	5.11E+04	48.3982	0.3289	5.14E+04	50.8746	0.2939	5.15E+04	106.8068	0.2500
	q-PCKMeans (IG)	5.24E+04	52.5752	0.0088	5.25E+04	58.1897	0.0088	5.28E+04	142.3847	0.0899
Land mine n = 338 d = 3 k=5	cop-kmeans	32.77	0.2102	0.0000	No solution found			No solution found		
	mpckmeans	32.29	0.4613	0.0485	63.43	0.1907	0.0521	57.67	0.1868	0.0143
	pckmeans	32.12	0.3310	0.0000	58.78	0.1316	0.0888	46.36	0.0869	0.0387
	q-PCKMeans (CA)	26.96	121.1480	0.0000	36.64	415.2133	0.4405	43.69	130.9266	0.0000
	q-PCKMeans (IG)	27.48	183.9324	0.0000	51.11	329.8362	0.1071	50.79	350.3663	0.0536
Moons_2 n = 400 m = 2 k=2	cop-kmeans	No solution found			No solution found			No solution found		
	mpckmeans	474.23	0.2361	0.1210	525.55	0.1571	0.0265	490.45	2.6968	0.0175
	pckmeans	453.81	0.0976	0.0360	434.85	0.1160	0.0255	438.67	0.1660	0.0225
	q-PCKMeans (CA)	373.35	37.3382	0.0000	368.07	46.2129	0.0000	356.25	66.6683	0.1017
	q-PCKMeans (IG)	381.59	33.1576	0.0000	381.98	31.0663	0.0000	401.28	42.2272	0.0050
Monk_2 n = 432 d = 6 k=2	cop-kmeans	No solution found			No solution found			No solution found		
	mpckmeans	1.52E+03	0.1466	0.0542	1.52E+03	0.1934	0.0523	1.52E+03	0.6113	0.0556
	pckmeans	1.55E+03	0.1035	0.0528	1.55E+03	0.1043	0.0523	1.54E+03	0.0810	0.0523
	q-PCKMeans (CA)	1.52E+03	67.4376	0.2809	1.52E+03	55.9744	0.2377	1.53E+03	67.4376	0.2670
	q-PCKMeans (IG)	5.24E+04	52.5752	0.0088	5.25E+04	58.1897	0.0088	5.28E+04	142.3847	0.0899
An blobs n = 500 m = 2 k=3	cop-kmeans	169.61	3.6107	0.0000	157.62	2.7168	0.0000	166.13	5.7878	0.0000
	mpckmeans	153.43	0.3009	0.0000	353.09	0.2499	0.0040	329.81	4.4710	0.0080
	pckmeans	168.21	0.1743	0.0000	200.72	0.1640	0.0024	218.25	0.1649	0.0120
	q-PCKMeans (CA)	153.44	92.2314	0.0000	153.44	123.9325	0.0000	153.44	84.2249	0.0000
	q-PCKMeans (IG)	154.90	73.9097	0.0000	153.94	82.6313	0.0000	153.90	77.6430	0.0000
Vd blobs n = 600 m = 2 k=3	cop-kmeans	No solution found			No solution found			No solution found		
	mpckmeans	386.47	0.3158	0.0113	637.08	0.3427	0.0277	575.47	2.0543	0.0120
	pckmeans	415.18	0.2596	0.0000	448.27	0.3463	0.0323	439.31	0.3421	0.0167
	q-PCKMeans (CA)	368.67	83.7926	0.0000	356.71	141.9823	0.0800	358.01	93.3406	0.0633
	q-PCKMeans (IG)	370.68	90.5862	0.0000	410.21	104.0244	0.0089	419.42	118.6594	0.0033
Raisins n = 900 m = 7 k=3	cop-kmeans	No solution found			No solution found			No solution found		
	mpckmeans	1.55E+12	0.8031	0.0742	1.99E+12	0.6772	0.0289	1.88E+12	8.6050	0.0167
	pckmeans	1.78E+12	0.4880	0.0371	1.76E+12	0.4460	0.0291	1.86E+12	0.5017	0.0293
	q-PCKMeans (CA)	1.45E+12	45.8665	0.0000	1.28E+12	77.6761	0.1481	1.29E+12	102.1515	0.3802
	q-PCKMeans (IG)	1.38E+12	41.7418	0.0000	1.49E+12	75.7384	0.0000	1.44E+12	104.7233	0.1016

Table 5: Clustering evaluation metrics on solutions of datasets under different constraint settings.

METRICS	CONSTRAINTS	IRIS $k = 3$	SEEDS $k = 3$	HABERMAN $k = 2$	MOONS $k = 2$	SPIRAL $k = 2$	LAND_MINE $k = 5$
ARI	MSSC	0.5912	0.6890	(0.0015)	0.4977	(0.0005)	0.0782
	Q-PCKMEANSW (ML)	0.6051	0.7208	0.0070	0.5864	0.0054	0.0986
	Q-PCKMEANSW (CL)	0.5941	0.6890	0.0097	0.5362	(0.0017)	0.0790
	Q-PCKMEANSW (ML+CL)	0.6051	0.7116	0.0058	0.5560	0.0054	0.0905
AMI	MSSC	0.6302	0.6567	(0.0006)	0.3971	(0.0004)	0.1216
	Q-PCKMEANSW (ML)	0.6547	0.6857	0.0060	0.4791	0.0039	0.1402
	Q-PCKMEANSW (CL)	0.6428	0.6567	0.0130	0.4321	(0.0013)	0.1219
	Q-PCKMEANSW (ML+CL)	0.6547	0.6860	0.0043	0.4506	0.0039	0.1306
PURITY	MSSC	0.8067	0.8048	0.7353	0.7500	0.5133	0.3017
	Q-PCKMEANSW (ML)	0.8200	0.8952	0.7353	0.8833	0.5467	0.3550
	Q-PCKMEANSW (CL)	0.8133	0.8810	0.7353	0.8667	0.5200	0.3462
	Q-PCKMEANSW (ML+CL)	0.8200	0.8905	0.7353	0.8733	0.5467	0.3462

Table 6: SSE with respect to different backend and number of shots from 256 to 2048

CONSTRAINT	BACKEND	IRIS				SEEDS				MONK_2			
		256	512	1024	2048	256	512	1024	2048	256	512	1024	2048
CL	IDEAL	131.21	137.46	138.29	107.73	861.91	855.96	853.45	781.90	1547.44	1543.70	1547.80	1540.06
	FLIMAV2	156.64	156.31	131.88	131.57	883.29	882.59	851.02	847.75	1548.29	1545.62	1547.15	1545.67
	FJAKARTAV2	143.94	145.99	132.25	133.54	861.50	832.84	860.74	802.59	1547.84	1548.82	1545.71	1548.30
	FBROOKLYNV2	147.05	142.92	142.44	127.66	865.11	841.89	811.02	862.77	1549.52	1549.39	1547.02	1547.87
ML	IDEAL	176.31	190.65	168.43	138.71	969.90	920.77	900.90	882.40	1547.73	1548.07	1548.06	1540.88
	FLIMAV2	178.23	168.47	191.07	166.91	973.36	926.03	918.26	891.71	1548.90	1549.37	1546.63	1548.98
	FJAKARTAV2	190.85	168.79	170.90	190.57	940.56	976.28	915.39	937.48	1548.63	1549.19	1548.73	1548.47
	FBROOKLYNV2	184.96	190.02	172.68	178.03	896.85	910.17	951.63	953.02	1546.19	1550.41	1549.18	1545.93
BOTH	IDEAL	153.51	153.09	161.60	130.27	809.92	838.85	814.06	770.84	1543.12	1545.29	1542.75	1540.71
	FLIMAV2	160.46	176.15	160.32	141.74	849.84	848.48	831.94	844.48	1543.00	1545.00	1546.20	1549.23
	FJAKARTAV2	160.90	161.99	148.97	150.64	830.13	887.40	837.10	807.61	1545.82	1545.38	1544.11	1546.30
	FBROOKLYNV2	170.90	174.86	148.71	153.15	858.02	872.79	831.61	826.52	1547.33	1547.11	1547.47	1550.87

D.5 Robustness to Noise

To comprehensively evaluate the robustness of our proposed Q-PCKMEANS algorithm under realistic quantum hardware conditions, we performed a systematic noise-sensitivity analysis using IBM’s AerSimulator with noise models derived from one ideal simulator and three representative IBM-Q fake backends. We considered ideal (noiseless AerSimulator) and three hardware-emulated backends with increasing qubit capacities: `FakeLimaV2` (7 qubits), `FakeJakartaV2` (27 qubits), and `FakeBrooklynV2` (65 qubits), in order to capture varying degrees of connectivity and coherence-time heterogeneity. For each configuration, we varied the number of measurement shots across four levels (256, 512, 1024, and 2048) to analyze statistical convergence and its impact on clustering quality. Across all IBM noise models tested, increasing the shot budget systematically reduces the SSE. From 256 shots where SSE can be up to approximately 20 percent above the ideal baseline, doubling the number of measurements reduces this gap by roughly one-third; quadrupling them to 1,024 shots brings the residual overhead into the single-digit-percent range. A further increase to 2,048 shots yields only marginal additional gains, signaling that hardware noise rather than sampling noise now sets the error floor. Although the overall trend is downward, minor non-monotonic variations occur for specific backend-dataset pairs. For example, an increase in SSE for `FakeJakartaV2` on `Seeds` when moving from 256 to 1,024 shots, reflecting statistical fluctuations. Device-level differences, such as the deeper circuits on the 65-qubit `FakeBrooklynV2` backend, shift the performance plateau by only a few percent. In practice, these observations indicate that a budget of one to two thousand shots suffices to keep noise-induced overheads both small and stable across the evaluated backends and datasets.

D.6 Real Hardware Implementation

We decided not to test our algorithm on real hardware, since current NISQ devices are composed of noisy and error-prone qubits, which makes them ill-suited for reliable clustering experiments on real hardware (Bharti et al., 2022). Median two-qubit error rates remain about 0.6%, so a depth-1 QAOA circuit with $\geq 10^3$ entangling gates would succeed with probability $< 10^{-3}$ per shot, rendering statistical comparisons meaningless without prohibitively many repetitions (Xue et al., 2021). Moreover, current devices offer only tens to a few hundred qubits, which severely limits the dimensionality and dataset sizes that can be encoded for clustering. Consequently, we emulate hardware noise with calibrated AerSimulator models, an established proxy that preserves the qualitative behaviour of today’s devices while deferring physical runs until processors with materially lower gate errors and higher qubit counts become available.

D.7 Societal Impact of q-PCKMeans

q-PCKMeans holds promise for accelerating data-driven discovery in domains such as genomics, precision medicine, and materials design, where early identification of meaningful subgroups can lead to improved diagnostic tools and targeted therapies. However, similar to classical k -means clustering, q-PCKMeans may reproduce or amplify existing biases present in the input data if fairness considerations are overlooked. Deployments that ignore fairness risks could inadvertently result in differential outcomes across demographic groups. Fairness-aware variants of clustering, such as those balancing group costs (Backurs et al., 2019) or enforcing demographic constraints (Chierichetti et al., 2017), provide potential avenues for addressing such biases. Additionally, clustering sensitive or personal data at fine granularity introduces privacy risks, including possible re-identification through linkage attacks. Integrating differential privacy techniques, for example by adding calibrated Laplace noise to centroid updates based on clustering objective sensitivity (Dwork et al., 2006), represents a direction that could mitigate these risks. Nonetheless, the effectiveness and practical implementation of fairness and privacy techniques in quantum-assisted clustering remain open questions, given the current state of quantum machine learning. This discussion serves primarily as a disclaimer, highlighting known risks from classical clustering methods and identifying future research opportunities in quantum clustering contexts.

E Penalty Weight λ

Across both easy (Block A) and hard (Block B) instances, all three constraint types (`m1`, `c1` and `both`) and five random seeds, we observe a broad plateau in the penalty range $0.05 \leq \lambda \leq 5$: the sum-of-squared-errors (SSE) deviates by less than 3 % from the reference value, and even an extreme choice of $\lambda = 50$ worsens SSE by only about 1.5 %. The number of ML/CL violations decreases as λ grows, while wall-clock time fluctuates modestly (around 10–12 s) and logical-qubit usage stays within 178–186 qubits (variation $\leq 5\%$), so tuning λ adds no meaningful hardware cost (see Fig. 6). This empirical plateau aligns with the additive-improvement window predicted by Theorem 8,

$$\lambda_* \lesssim \lambda \lesssim \frac{\bar{\eta}|S|}{2\kappa}.$$

Boxplots in Fig. 7 show that the medians and interquartile ranges of SSE overlap almost perfectly across more than two orders of magnitude in λ . Hence, within the datasets and constraint densities explored, precise tuning of λ in the range 0.05–5 is unnecessary to achieve near-optimal accuracy with stable runtime and consistently low constraint violations.

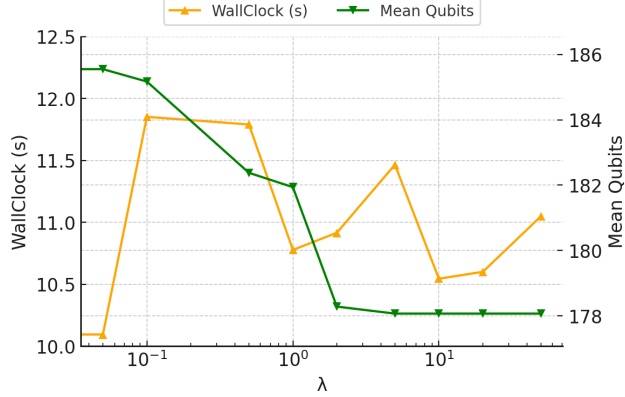


Figure 6: Wall-clock time (orange triangles, left axis) and logical-qubit usage (green triangles, right axis) versus penalty weight λ (log scale). Both metrics vary by less than 5 % across the sweep, confirming that adjusting λ incurs no additional resource cost.

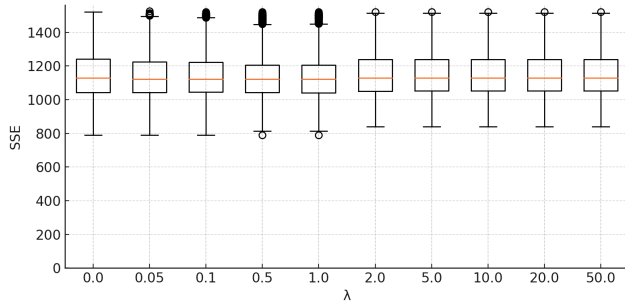


Figure 7: Boxplots of SSE distributions for each tested λ value (categorical axis). The nearly perfect overlap of medians and interquartile ranges across $\lambda \in \{0.05, 0.1, 0.5, 1, 2, 5, 10, 20, 50\}$ corroborates the predicted performance plateau.

References

Aloise, D., Deshpande, A., Hansen, P., and Popat, P. (2009). Np-hardness of euclidean sum-of-squares clustering. *Machine Learning*, 75(2):245–248.

Arute, F., Arya, K., Babbush, R., Bacon, D., Bardin, J. C., Barends, R., Biswas, R., Boixo, S., Brandao, F. G., Buell, D. A., et al. (2019). Quantum supremacy using a programmable superconducting processor. *Nature*, 574(7779):505–510.

Backurs, A., Indyk, P., Onak, K., Schieber, B., Vakilian, A., and Wagner, T. (2019). Scalable fair clustering. In *International conference on machine learning*, pages 405–413. PMLR.

Barenco, A., Bennett, C. H., Cleve, R., DiVincenzo, D. P., Margolus, N., Shor, P., Sleator, T., Smolin, J. A., and Weinfurter, H. (1995). Elementary gates for quantum computation. *Physical review A*, 52(5):3457.

Basu, S., Banerjee, A., and Mooney, R. J. (2004). Active semi-supervision for pairwise constrained clustering. In *Proceedings of the 2004 SIAM International Conference on Data Mining (SDM)*, pages 333–344. Society for Industrial and Applied Mathematics.

Basu, S., Davidson, I., and Wagstaff, K., editors (2008). *Constrained Clustering: Advances in Algorithms, Theory, and Applications*. Chapman and Hall/CRC, New York, n.d. edition.

Baumann, P. (2020). A binary linear programming-based k-means algorithm for clustering with must-link and cannot-link constraints. In *2020 IEEE international conference on industrial engineering and engineering management (IEEM)*, pages 324–328. IEEE.

Baumann, P. and Hochbaum, D. S. (2024). An algorithm for clustering with confidence-based must-link and cannot-link constraints. *INFORMS Journal on Computing*, 34(1).

Bharti, K., Cervera-Lierta, A., Kyaw, T. H., Haug, T., Alperin-Lea, S., Anand, A., Degroote, M., Heimonen, H., Kottmann, J. S., Menke, T., et al. (2022). Noisy intermediate-scale quantum algorithms. *Reviews of Modern Physics*, 94(1):015004.

Bhattacharya, A., Jaiswal, R., and Kumar, A. (2018). Faster algorithms for the constrained k-means problem. *Theory of computing systems*, 62(1):93–115.

Bilenko, M., Basu, S., and Mooney, R. J. (2004). Integrating constraints and metric learning in semi-supervised clustering. In *Proceedings of the twenty-first international conference on Machine learning*, page 11.

Boros, E., Hammer, P. L., and Tavares, G. (2007). Local search heuristics for quadratic unconstrained binary optimization (qubo). *Journal of Heuristics*, 13(2):99–132.

Braverman, V., Feldman, D., Lang, H., Statman, A., and Zhou, S. (2021). Efficient coresets constructions via sensitivity sampling. In *Asian Conference on Machine Learning*, pages 948–963. PMLR.

Brieden, A., Gritzmann, P., and Klemm, F. (2017). Constrained clustering via diagrams: A unified theory and its application to electoral district design. *European Journal of Operational Research*, 263(1):18–34.

Chen, T., Ray, A., Seshadri, A., Herman, D., Bach, B., Deshpande, P., Som, A., Kumar, N., and Pistoia, M. (2025). Provably faster randomized and quantum algorithms for k -means clustering via uniform sampling. *arXiv preprint arXiv:2504.20982*.

Chierichetti, F., Kumar, R., Lattanzi, S., and Vassilvitskii, S. (2017). Fair clustering through fairlets. *Advances in neural information processing systems*, 30.

Chumpitaz-Flores, P., Duong, M., Heredia, C., and Hua, K. (2025a). A scalable global optimization algorithm for constrained clustering. *arXiv preprint arXiv:2510.22519*.

Chumpitaz-Flores, P., Duong, M., Mao, Y., and Hua, K. (2025b). qc-kmeans: A quantum compressive k-means algorithm for nisq devices. *arXiv preprint arXiv:2510.22540*.

Cohen, E., Senderovich, A., and Beck, J. C. (2020). An ising framework for constrained clustering on special purpose hardware. In *International Conference on Integration of Constraint Programming, Artificial Intelligence, and Operations Research*, pages 130–147. Springer.

Davidson, I. and Ravi, S. S. (2005). Clustering with constraints: Feasibility issues and the k-means algorithm. In *Proceedings of the 2005 SIAM International Conference on Data Mining (SDM)*, pages 138–149. Society for Industrial and Applied Mathematics.

Deutsch, D. (1985). Quantum theory, the church–turing principle and the universal quantum computer. *Proceedings of the Royal Society of London. A. Mathematical and Physical Sciences*, 400(1818):97–117.

Dua, D. and Graff, C. (2017). Uci machine learning repository.

Dwork, C., McSherry, F., Nissim, K., and Smith, A. (2006). Calibrating noise to sensitivity in private data analysis. In *Theory of cryptography conference*, pages 265–284. Springer.

Egger, D. J., Mareček, J., and Woerner, S. (2021). Warm-starting quantum optimization. *Quantum*, 5:479.

Glover, F., Kochenberger, G., and Du, Y. (2019). A tutorial on formulating and using qubo models.

Guns, T., Dao, T.-B.-H., Vrain, C., and Duong, K.-C. (2016). Repetitive branch-and-bound using constraint programming for constrained minimum sum-of-squares clustering. In *Proceedings of the Twenty-second European Conference on Artificial Intelligence*, pages 462–470, NLD. IOS Press.

Hadfield, S., Wang, Z., O’gorman, B., Rieffel, E. G., Venturelli, D., and Biswas, R. (2019). From the quantum approximate optimization algorithm to a quantum alternating operator ansatz. *Algorithms*, 12(2):34.

Hao, T., He, Z., Shaydulin, R., Larson, J., and Pistoia, M. (2024). End-to-end protocol for high-quality qaoa parameters with few shots. *arXiv preprint arXiv:2408.00557*.

Harrow, A. W. (2020). Small quantum computers and large classical data sets. *arXiv:2004.00026 [quant-ph]*.

Huang, H., Cheng, Y., and Zhao, R. (2008). A semi-supervised clustering algorithm based on must-link set. In Tang, C., Ling, C. X., Zhou, X., Cercone, N. J., and Li, X., editors, *Advanced Data Mining and Applications*, pages 492–499, Berlin, Heidelberg. Springer.

Huang, L., Li, J., Lu, P., and Wu, X. (2025). Coresets for constrained clustering: General assignment constraints and improved size bounds. In *Proceedings of the 2025 Annual ACM-SIAM Symposium on Discrete Algorithms (SODA)*, pages 4732–4782. SIAM.

Jain, A. K. (2010). Data clustering: 50 years beyond k-means. *Pattern Recognition Letters*, 31(8):651–666.

Kumari, M. and Ghose, S. (2018). Quantum-classical correspondence in the vicinity of periodic orbits. *Physical Review E*, 97(5):052209.

Könz, M. S., Lechner, W., Katzgraber, H. G., and Troyer, M. (2021). Embedding overhead scaling of optimization problems in quantum annealing. *PRX Quantum*, 2(4).

Lloyd, S. (1982). Least squares quantization in pcm. *IEEE Transactions on Information Theory*, 28(2):129–137.

McQueen, J. B. (1967). Some methods of classification and analysis of multivariate observations. In *Proc. of 5th Berkeley Symposium on Math. Stat. and Prob.*, pages 281–297.

Mirkarimi, P., Hoyle, D. C., Williams, R., and Chancellor, N. (2024a). Experimental demonstration of improved quantum optimization with linear ising penalties. *New Journal of Physics*, 26(10):103005.

Mirkarimi, P., Shukla, I., Hoyle, D. C., Williams, R., and Chancellor, N. (2024b). Quantum optimization with linear ising penalty functions for customer data science. *Phys. Rev. Res.*, 6:043241.

Nghiêm, N.-V.-D., Vrain, C., Dao, T.-B.-H., and Davidson, I. (2020). Constrained clustering via post-processing. In *Discovery Science: 23rd International Conference, DS 2020, Thessaloniki, Greece, October 19–21, 2020, Proceedings*, pages 53–67, Berlin, Heidelberg. Springer-Verlag.

Nielsen, M. A. and Chuang, I. L. (2010). *Quantum computation and quantum information*. Cambridge university press.

Piccialli, V., Russo Russo, A., and Sudoso, A. M. (2022). An exact algorithm for semi-supervised minimum sum-of-squares clustering. *Computers & Operations Research*, 147.

Preskill, J. (2018). Quantum computing in the nisq era and beyond. *Quantum*, 2:79.

Qu, F., Erfani, S. M., and Usman, M. (2022). Performance analysis of coresets selection for quantum implementation of k-means clustering algorithm.

Richoux, F., Baffier, J.-F., and Codognet, P. (2023). Learning qubo models for quantum annealing: A constraint-based approach. In *International Conference on Computational Science*, pages 153–167. Springer.

Rutayisire, T., Yang, Y., Lin, C., and Zhang, J. (2011). A modified cop-kmeans algorithm based on sequenced cannot-link set. In Yao, J., Ramanna, S., Wang, G., and Suraj, Z., editors, *Rough Sets and Knowledge Technology*, pages 217–225, Berlin, Heidelberg. Springer.

Saiphet, J., Suwanna, S., Chotibut, T., and Chantasri, A. (2021). Quantum approximate optimization and k-means algorithms for data clustering. In *Journal of Physics: Conference Series*, volume 1719, page 012100. IOP Publishing.

Schmidt, M. and Wargalla, J. (2021). Coresets for constrained k-median and k-means clustering in low dimensional euclidean space.

Seong, M. and Park, D. K. (2025). Hamiltonian formulations of centroid-based clustering. *Frontiers in Physics*, 13:1544623.

Späth, H. (1980). *Cluster Analysis Algorithms for Data Reduction and Classification of Objects*. E. Horwood, n.d., n.d. edition.

Tan, W., Yang, Y., and Li, T. (2010). An improved cop-kmeans algorithm for solving constraint violation. In *Computational Intelligence: Foundations and Applications*, pages 690–696. World Scientific.

Tian, T., Zhang, J., Lin, X., Wei, Z., and Hakonarson, H. (2021). Model-based deep embedding for constrained clustering analysis of single cell rna-seq data. *Nature Communications*, 12(1):1873.

Tomesh, T., Gokhale, P., Anschuetz, E. R., and Chong, F. T. (2020). Coreset Clustering on Small Quantum Computers. arXiv:2004.14970 [quant-ph].

Tomesh, T., Gokhale, P., Anschuetz, E. R., and Chong, F. T. (2021a). Coreset clustering on small quantum computers. *Electronics*, 10(14):1690.

Tomesh, T., Gokhale, P., Anschuetz, E. R., and Chong, F. T. (2021b). Coreset clustering on small quantum computers. *Electronics*, 10(14):1690.

Wagstaff, K., Cardie, C., Rogers, S., and Schrödl, S. (2001). Constrained k-means clustering with background knowledge. In *Proceedings of the Eighteenth International Conference on Machine Learning*, pages 577–584, San Francisco, CA, USA. Morgan Kaufmann Publishers Inc.

Xiong, C., Johnson, D. M., and Corso, J. J. (2016). Active clustering with model-based uncertainty reduction. *IEEE transactions on pattern analysis and machine intelligence*, 39(1):5–17.

Xu, J. and Lange, K. (2019). Power k-means clustering. In *Proceedings of the 36th International Conference on Machine Learning*, pages 6921–6931, Berlin, Heidelberg. PMLR.

Xu, Q., desJardins, M., and Wagstaff, K. L. (2005). Active constrained clustering by examining spectral eigenvectors. In *International Conference on Discovery Science*, pages 294–307. Springer.

Xue, C., Chen, Z.-Y., Wu, Y.-C., and Guo, G.-P. (2021). Effects of quantum noise on quantum approximate optimization algorithm. *Chinese Physics Letters*, 38(3):030302.

Yang, Y., Zhang, K., and Fan, Y. (2022). Analyzing firm reports for volatility prediction: A knowledge-driven text-embedding approach. *INFORMS Journal on Computing*, 34(1):522–540.

Yung, C. and Usman, M. (2024). Clustering by contour coresnet and variational quantum eigensolver. *Advanced Quantum Technologies*, 7(8):2300450.

Zaiou, A., Bennani, Y., Matei, B., and Hibti, M. (2021). Balanced k-means using quantum annealing. In *2021 IEEE Symposium Series on Computational Intelligence (SSCI)*, pages 1–7. IEEE.